Crustal properties beneath the northeastern United States shaped by past tectonic processes

James R. Bourke[1]*, Maureen D. Long[2], Frederik Link[2], Paul Karabinos[3], Laura Webb[4], Yantao Luo[2], Kimberly Espinal[2], Roberto Masis Arce[1] and Yiran Li[5]

[1]Rutgers University New Brunswick, New Brunswick, NJ, USA

[2]Department of Earth and Planetary Sciences, Yale University, New Haven, USA

[3]Department of Geosciences, Williams College, Williamstown, MA, USA

[4]Department of Geography and Geosciences, University of Vermont, Bington, VT, USA

[5]Department of Geological Sciences and Environmental Studies, Binghamton University, Binghamton, NY, USA

JRB, 0000-0003-1399-5628; MDL, 0000-0003-1936-3840; FL, 0000-0003-1639-0093; PK, 0000-0003-1611-1971; LW, 0000-0002-0597-5793; YL, 0000-0001-5165-3640; KE, 0000-0002-0864-8106; RMA, 0009-0003-3772-3640

*Correspondence: jrb370@eps.rutgers.edu

Abstract: Constraints on the thickness, transitional boundaries, and composition of Earth's crust are pivotal in studying its formation and evolution. We use data from 132 seismic installations throughout the northeastern US to explore how tectonic events, such as orogenesis and rifting, have altered the crust of the northeastern US and southeastern Canada, and to distinguish between Laurentia and the Appalachian terranes. We include data from seismic installations from the NEST and SEISConn experiments, spanning the Laurentia–Appalachian boundary, and present estimates of crustal thickness, V_p/V_s, and thickness of the transition between crustal and mantle rocks using Ps receiver functions. We find some first-order differences between Laurentia and Appalachian terranes, with Laurentia exhibiting thicker crust (*c.* 39 v. *c.* 33 km) and a broader crust–mantle transition thickness (*c.* 3 v. <1.5 km). Average V_p/V_s values are similar between Laurentia (*c.* 1.77) and Appalachian terranes (*c.* 1.74); however, we identify anomalous V_p/V_s in a few regions, including high V_p/V_s around the Adirondack Mountains and low V_p/V_s in southern New England. The southern New England region is also anomalous in terms of its systematically thinner crust and sharper crust–mantle transition, which may be a consequence of the formation and collapse of the Acadian altiplano during the mid-to-late Paleozoic.

Supplementary material: Supplemental materials are available at https://figshare.com/articles/figure/Revised_Supplement_File/25934686

Geological and tectonic background

The eastern North American margin (Fig. 1) records two complete supercontinent cycles (Wilson 1966). The Mesoproterozoic Grenville orogenies culminated in the formation of the supercontinent Rodinia (e.g. Rivers 2015), and the later Paleozoic Appalachian orogenies amalgamated the supercontinent Pangaea (Hatcher 2010). The assembly of Rodinia from 1.3 to 0.9 Ga (e.g. Li *et al.* 2008) was piecewise, first with the accretion of island arc terranes by the Elzevirian and Shawinigan orogenies, followed by the continent–continent Ottawan Orogeny. From 1.3 to 1 Ga the formation, emplacement and re-working of Adirondack lithosphere of New York occurred contemporaneously with the assembly of Rodinia. The Adirondacks Mountains comprise Mesoproterozoic metasedimentary and metaigneous rocks from the Grenville orogeny (Rivers 2008; Chiarenzelli *et al.* 2010; McLelland *et al.* 2013) and are thought to be actively uplifting by *c.* 1 mm/year today (Isachsen 1975), perhaps owing to buoyancy of the asthenosphere beneath (Yang and Gao 2018).

The supercontinent of Rodinia began to break up owing to rifting between 750 and 700 Ma (Li *et al.* 2008; Hatcher 2010), forming the ancient continent Laurentia. Pulses of failed rifting around *c.* 735 Ma are inferred from features in the southern and central Appalachians (Hatcher 2005), with the northern Appalachians experiencing a later onset of rifting. Successful rifting initiated along the eastern

From: Ben-Mansour, W., Schiffer, C. and Gradmann, S. (eds) *Structure and Evolution of Laurussian Orogens in Europe and North America from Geophysical Investigations*. Geological Society, London, Special Publications, **557**, https://doi.org/10.1144/SP557-2024-30

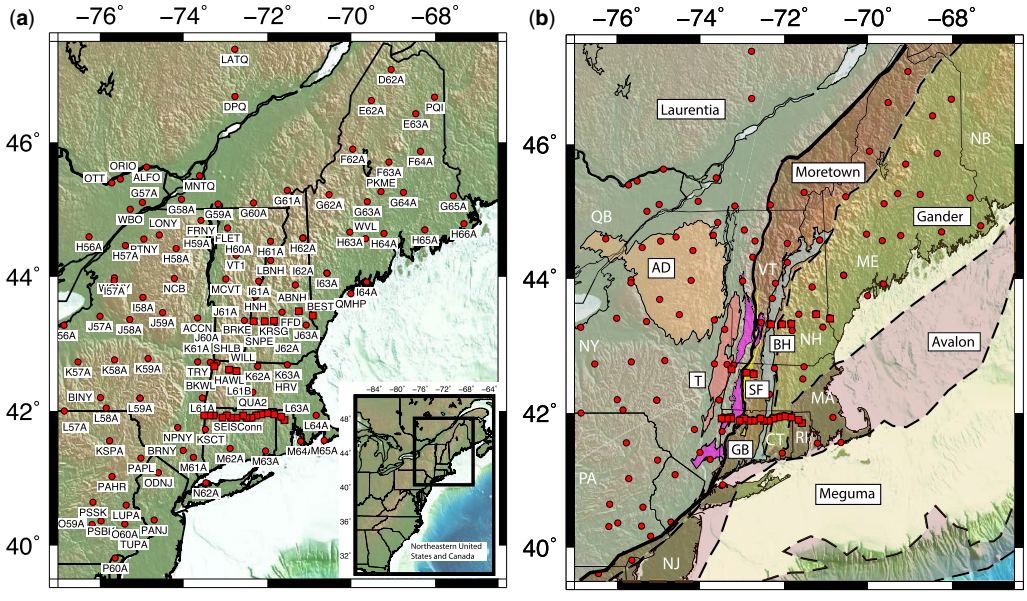

Fig. 1. (**a**) Regional map of New England and southeastern Canada. Red circles are locations of the seismic stations used in this study, with station names shown. SEISConn represents 15 stations of the temporary seismic network XP, with the station naming convention CS01–CS15. (**b**) Tectonic map of New England and southeastern Canada. Black lines are modified from Lund *et al.* (2015). Solid black line represents the boundary between Laurentia and the Appalachian terranes, with stippled black lines corresponding to boundaries between individual Appalachian terranes. Background shows GMRT topography (Ryan *et al.* 2009). BH, Bronson Hill Arc; T, Taconic Ranges; SF, Shelburne Falls Arc; GB, Grenville Basement massifs (blue); AD, Grenville Basement of Adirondack Mountains.

Laurentian margin at 570–555 Ma (Cawood *et al.* 2001), which evolved as a passive continental margin until the Early Ordovician (Karabinos *et al.* 2017).

The Appalachian Orogenies began *c.* 485–480 Ma (Aiken 2018), with four significant accretionary events affecting the northern Appalachians (Fig. 1b), beginning with ophiolite or mantle lenses emplacement into the continental rocks between 490 and 457 Ma (Julien and Hubert 1975; Whitehead *et al.* 1995, 1996; Tremblay *et al.* 2011). The first event, the Taconic orogeny, involved the collision of the Moretown terrane with Laurentia by means of eastward-dipping subduction (Macdonald *et al.* 2014; Karabinos *et al.* 2017). During Taconic orogenesis, the polarity of subduction reversed from east-dipping to west-dipping beneath Laurentia (Macdonald *et al.* 2014; Karabinos *et al.* 2017). The western boundary of the Moretown terrane coincides with the suture between Laurentian and Appalachian terranes (Fig. 1b). The second accretionary event, the Salinic Orogeny, primarily involved continent–continent convergence as Ganderia was accreted onto the eastern Laurentian margin (van Staal *et al.* 2009). During the third accretionary event, the Acadian orogeny, Avalon collided with Laurentia, causing widespread overprinting of the geological record of the previous orogenic events. Accretion of Meguma may have triggered the Neoacadian orogeny (van Staal *et al.* 2009), although this terrane is not clearly recognized in our study area. The culminating phase of Appalachian orogenesis was the Alleghenian orogeny when Gondwana collided with Laurentia, closing the Iapetus Ocean and forming the supercontinent of Pangaea (Hatcher 2010). This was followed by Mesozoic rifting and the break-up of Pangaea *c.* 200 Ma (Withjack and Schlische 2005; Hatcher 2010; Mazza *et al.* 2017). Additionally, significant crustal alteration probably occurred to accommodate the expressions of continental magmatism dated to *c.* 124 Ma, often associated with edge-driven convection (Cooper Boemmels 2020) and the passing of the North American continent over the Great Meteor Hotspot *c.* 125–100 Ma (Eaton and Frederiksen 2007; Kinney *et al.* 2021).

Previous seismological studies of northeastern US crust

Before the deployment of the USArray Transportable Array component of EarthScope (IRIS Transportable Array 2003), constraints on crustal

structure beneath the northeastern US came from local active source (e.g. Ando *et al.* 1984; Hughes and Luetgert 1991; Hughes *et al.* 1993; Musacchio *et al.* 1997) and passive source (e.g. Levin *et al.* 1995*a*, *b*; Viegas *et al.* 2010) studies that, while valuable, suffered from sparse seismic station coverage. The EarthScope initiative greatly increased the spatial density of the available seismic installations, covering the entire continental US with a 70 × 70 km grid. USArray data have enabled numerous studies of the nature of the crust and upper mantle beneath the northeastern US and surrounding regions (e.g. Levin *et al.* 2017, 2018; C. Li *et al.* 2018, 2020, 2023; Yang and Gao 2018; Y. Li *et al.* 2019, 2021; Bagherpur Mojaver and Darbyshire 2022; Link *et al.* 2022). Specifically, Li *et al.* (2018, 2020) provided evidence for a first-order transition in crustal structure from the Appalachian terranes to the Grenville belt of Laurentia, with substantially thicker (+10–15 km) crust beneath Laurentia. The detailed characteristics of this crustal transition were further delineated using data from the temporary seismic deployments, SEISConn and NEST, which sampled across the Appalachian–Laurentian suture of Connecticut, Massachusetts and Vermont with *c.* 10–15 km station spacing (Long and Aragon 2020; Luo *et al.* 2021, 2023*a*, *b*; Goldhagen *et al.* 2022; Masis *et al.* 2024). Levin *et al.* (2017) used data from a similar temporary seismic deployment with dense station spacing across the Superior Craton, Grenville Province and Appalachian terranes in northern Maine and southeastern Canada. They reported Grenville crust to be generally thicker than Appalachian crust; however, they noted that the Appalachian crust had much more variation in thickness.

The EarthScope Automated Receiver Survey (EARS; Crotwell and Owens 2005; IRIS, DMC 2010; Trabant *et al.* 2012), a publicly available data product that relies on EarthScope and other seismic data, produces automated estimates of crustal thickness and the ratio of P-wave (V_p) and S-wave (V_s) velocities (V_p/V_s). The EARS applies standardized receiver function processing and analysis, taking advantage of the timing of reverberated crustal multiples to estimate V_p/V_s. The EARS database includes all permanent stations used in our study.

Crustal characteristics: thickness, lithology and Moho sharpness

Several characteristics of continental crust are of interest to geologists because they can shed light on the processes through which crust formed and evolved through time. These include its thickness and lithology, as well as the nature of the transition from the crust to the underlying mantle. Estimates of present-day crustal thickness can provide insight into past tectonic processes such as orogenesis, rifting, erosion and exhumation. In combination with topography, crustal thickness reflects the nature of isostatic compensation and the crustal density. Estimates of the vertical extent of the crust–mantle transition, known as the Moho sharpness or thickness, can help us understand the degree of crustal reworking, modification and underplating over geological time (Levin *et al.* 2016, 2017).

Crustal lithology is another important indicator, although estimating lithology from seismological observables remains a challenge for seismology. Compressional wave velocity alone is not enough to distinguish rock types, owing to large overlaps of V_p for different lithologies (for example, a rock with a P-wave velocity of 5.8 km s^{-1} could be granite, quartzite or serpentinite; Holbrook *et al.* 1992). This challenge becomes more difficult when accounting for increased metamorphic grade and potentially mafic compositions in the deeper portions of the crust. Laboratory studies such as Holbrook *et al.* (1992), Christensen and Mooney (1995) and Christensen (1996) have provided measurements of seismic P and S wave velocity as a function of temperature and depth for crustal rocks. These studies have shown that the ratio of P and S wave velocities (V_p/V_s) shows stronger sensitivity for rock types and can be used to differentiate between silica-rich (felsic) rocks and silica-poor (mafic) rocks. Typically, felsic rocks have V_p/V_s of *c.* 1.7–1.77, whereas mafic and ultramafic rocks display higher V_p/V_s values of >1.8–1.88, and up to 2.0 for some lithologies (Christensen and Mooney 1995; Rudnick and Fountain 1995; Christensen 1996, 2004). Observational constraints on V_p/V_s from seismic data therefore allow for estimates of potential bulk crustal lithologies (e.g. Zhu and Kanamori 2000; Linkimer *et al.* 2010; Wagner *et al.* 2012; Levin *et al.* 2017).

Goals of this study

Our study combines both long-running and temporary seismic installations to investigate the crustal properties and structure of the New England Appalachians and adjacent Grenville belt. By incorporating dense transects of temporary seismic deployments (NEST and SEISConn), we significantly improve spatial precision of our interpretations, particularly across the suture between Laurentia and the accreted Moretown terrane. We present regional measurements of multitaper spectral correlated receiver function estimates (Park and Levin 2000) throughout New England, specifically taking advantage of the H-k stacking (Zhu and Kanamori 2000) to constrain crustal thickness and V_p/V_s. Additionally, we present a regional investigation of the thickness of the crust–mantle transition beneath the New England

using changes in converted pulse shape to delineate the sharpness of the Moho transition. Lastly, we compare our results with recent work by Chai *et al.* (2022), showing a discrepancy between their published results defining the Moho as 7.8 km s^{-1} P-wave velocity and the work presented here. We ensure consistency across our study region by following principles of uniformity in our methodology, data selection, processing and interpretation. The primary aim of this study was to delineate the differences in the properties of crustal thickness, V_p/V_s ratio and Moho transition thickness across the Grenville belt and the various accreted Appalachian terranes, and to interpret those differences in terms of past tectonic events and lithospheric evolution. We intend for our uniform and comprehensive dataset to be used by the community as a repository of information about the composition and architecture of the northeastern US crust. Our measurements shed new light on how geological processes, such as tectonic inheritance, orogenesis, orogenic collapse, terrane accretion, continental rifting and delamination, have influenced crustal evolution beneath this portion of the Appalachians.

Data

The seismological data used in this study are derived from publicly available sources for 132 continuously recording broadband seismic stations throughout our study region (Fig. 1a). This dataset includes stations from a variety of permanent and temporary seismic networks: Canadian National Seismograph Network (CN), Global Seismograph Network (IU), Lamont–Doherty Cooperative Seismographic Network (LD), Central and Eastern US Network (N4), New England Seismic Network (NE), Pennsylvania State Seismic Network (PE), Portable Observatories for Lithospheric Analysis and Research Investigating Seismicity (POLARIS; PO), USArray Transportable Array (TA), United States National Seismic Network (US), Deep Structure of Three Continental Sutures in Eastern North America (X8), New England Seismic Transects (NEST; 7O), and Seismic Experiment for Imaging Structure beneath Connecticut (SEISConn; XP). All data are accessible via the EarthScope SAGE (Seismological Facility for the Advancement of Geoscience) data centre (https://ds.iris.edu/ds/nodes/dmc/data/). Data were recorded between 2008 and 2023 with varying recording durations; for example, certain temporary stations have recorded for just over a year (e.g. 7O: BBVT), while other stations have recorded more than 10 years of high-quality data (e.g. US: BINY)

Our study focuses on three-component records for first arriving compressional waves (P) from teleseismic earthquakes. In total, we incorporate more than 20 241 events for P and P_{diff} (20–125°) and PKP (145°+) phases from earthquakes of magnitude of 5.7+. Records are first selected for a minimum signal-to-noise ratio of 2.5, with all records being visually inspected for coherent signals and the removal of excessively noisy traces. Station LD: BRNY has the greatest number of usable earthquake events with 497 and station 7O: BKWL has the least with 18 after inspection. The average number of earthquake records that were used to compute receiver functions per station is 152 (Table 1).

Methods

Receiver function computations

To make estimates of crustal thickness, V_p/V_s ratio and crust–mantle transition thickness at each station, we utilize the receiver function (RF) methodology (Ammon 1991; Langston 1977). Specifically, we use a multitaper correlation (MTC) algorithm for computing RFs (Park and Levin 2000) and implement a MTC RF harmonic decomposition method (Park and Levin 2016) to identify the parts of the RF signal that do not vary with direction. When a compressional wave (P) encounters a boundary with a contrast in impedance (the product of velocity and density), a portion of that P-phase energy is converted into a shear wave (P_s). Measurements of the delay times between the incident P-wave and the following P_s phases (including multiple reflections) allow for estimates of the depth and character of interfaces beneath the seismic station.

To compute RF traces, we rotate the seismograms into the ray-based (LQT) coordinate system; this coordinate transform suppresses the initial P-wave signal, which can otherwise dominate the first few seconds of the RFs. The L-component aligns with the particle motion of the incoming P-wave, while the Q-component records the converted P-to-SV phases created by impedance contrasts, and the T-component records converted P-to-SH phases created by directionally dependent properties such as anisotropy or dipping interfaces. The MTC method provides an estimate of RF uncertainty in the frequency domain, enabling RFs from different seismic events to be combined in a weighted-average RF estimate, rather than an unweighted stack. This method is more resistant to so-called signal-generated noise, which can contaminate RF estimates (Park and Levin 2000). This property allows MTC RF estimates to extend to frequencies well beyond 1 Hz, approaching the effective resolution of active-source deep-crustal seismic studies. However, the MTC method is limited to relatively shallow structures owing to an implicit frequency average from spectral correlation; this limits detection of P_s converted pulses to $T/2p$, where T is the

Table 1. Results of this study

Station	Latitude (deg)	Longitude (deg)	V_p/V_s	Thickness (km)	Moho transition (km)	Maximum frequency (Hz)	H-k quality	Number of EQs
ABNH	43.48	−71.25	1.804	34	2.02	1	2	77
ACCN	43.38	−73.67	1.816	43.5	1	2	3	216
ALFO	45.63	−74.88	1.75	39.5	2.17	1	3	43
BEST	43.42	−70.92	1.81	28	1	2	2	21
BINY	42.20	−75.99	1.738	48	1.1	2	3	348
BKWL	42.72	−73.37	1.87	37	N/A	N/A	2	18
BRKE	43.34	−72.34	1.834	32.5	0.65	3	3	77
BRNY	41.41	−74.01	1.774	42.5	4.2	0.5	2	497
CS01	41.94	−73.46	1.786	40.5	2.07	1	2	148
CS02	41.94	−73.34	1.618	49.5	2.63	1	1	63
CS03	41.95	−73.26	1.6	46	10.83	0.25	1	229
CS04	41.91	−73.07	1.768	28.5	8.46	0.25	2	74
CS05	41.94	−72.97	1.762	30.5	2.13	1	3	160
CS06	41.91	−72.87	1.678	31	1.2	2	3	147
CS07	41.90	−72.75	1.684	31	0.79	3	3	136
CS08	41.93	−72.60	1.702	31	0.77	3	3	140
CS09	41.90	−72.49	1.726	30.5	0.75	3	3	74
CS10	41.90	−72.37	1.72	31.5	1.13	2	3	70
CS11	41.94	−72.28	1.744	31.5	0.73	3	3	97
CS12	41.96	−72.12	1.726	33.5	0.75	3	3	108
CS13	41.97	−72.00	1.75	33.5	1.08	2	3	74
CS14	41.95	−71.84	1.78	34	1.04	2	3	189
CS15	41.89	−71.66	1.798	34.5	1.02	2	3	134
D62A	47.08	−69.05	1.852	36	1.91	1	2	132
DPQ	46.68	−72.78	1.99	30.5	0.82	2	2	100
E62A	46.62	−69.52	1.822	36.5	0.66	3	3	93
E63A	46.42	−68.46	1.732	34.5	0.74	3	3	136
F62A	45.90	−69.97	1.786	39	4.13	0.5	3	74
F63A	45.70	−69.10	1.726	35	1.12	2	3	132
F64A	45.86	−68.35	1.798	31.5	4.07	0.5	3	90
FFD	43.47	−71.65	1.732	32	4.44	0.5	3	102
FLET	44.72	−72.95	1.894	37.5	3.64	0.5	2	270
FRNY	44.84	−73.59	1.81	36	4.01	0.5	1	187
G57A	45.10	−74.99	1.768	37	0.71	3	3	60
G58A	45.15	−74.05	1.792	37.5	8.21	0.25	2	50
G59A	45.08	−73.18	1.774	38.5	8.4	0.25	2	20
G60A	45.10	−72.33	1.852	39.5	7.63	0.25	3	60
G61A	45.28	−71.53	1.852	32.5	3.81	0.5	1	59
G62A	45.22	−70.53	1.714	40.5	2.28	1	3	214
G63A	45.11	−69.62	1.678	36	4.79	0.5	3	57
G64A	45.25	−68.76	1.75	32.5	2.17	1	1	51
G65A	45.20	−67.56	1.708	33.5	0.77	3	2	100
H55A	44.55	−77.18	1.762	40	0.71	3	3	73
H56A	44.59	−76.26	1.744	41.5	0.73	3	3	44
H57A	44.46	−75.39	1.786	40.5	2.07	1	3	57
H58A	44.42	−74.18	1.816	41	0.66	3	3	73
H59A	44.65	−73.69	1.828	38	7.85	0.25	1	65
H60A	44.56	−72.70	1.684	41.5	2.38	1	2	59
H61A	44.52	−71.93	1.816	36	1	2	1	61
H62A	44.57	−71.16	1.69	36.5	0.79	3	3	288
H62A	44.57	−71.16	1.678	36.5	0.8	3	3	61
H63A	44.66	−70.04	1.702	38.5	2.31	1	3	41
H64A	44.64	−69.22	1.696	33.5	2.33	1	3	52
H65A	44.70	−68.25	1.738	32.5	0.73	3	3	62
H66A	44.79	−67.31	1.726	37	2.24	1	1	63
HAWL	42.61	−72.91	1.798	42.5	4.07	0.5	2	34

(*Continued*)

Table 1. *Continued*.

Station	Latitude (deg)	Longitude (deg)	V_p/V_s	Thickness (km)	Moho transition (km)	Maximum frequency (Hz)	H-k quality	Number of EQs
HNH	43.71	−72.29	1.948	31	1.71	1	1	221
HRV	42.51	−71.56	1.666	31	2.44	1	3	252
I55A	44.22	−77.68	1.648	25	1.25	2	1	72
I57A	43.94	−75.66	1.768	42	0.71	3	3	68
I58A	43.69	−74.97	1.744	43	0.73	3	2	64
I61A	43.93	−72.21	1.72	36.5	9.03	0.25	2	76
I62A	43.87	−71.34	1.744	36	1.09	2	3	200
I63A	44.05	−70.58	1.834	32.5	1.95	1	2	69
I63A	44.05	−70.58	1.804	33.5	4.04	0.5	3	202
I64A	43.92	−69.63	1.696	31	1.17	2	3	69
J56A	43.28	−76.86	1.702	49	2.31	1	1	66
J57A	43.41	−76.00	1.78	43	2.08	1	3	232
J58A	43.36	−75.29	1.81	42.5	2.01	1	1	69
J59A	43.46	−74.50	1.774	43	1.05	2	1	374
J60A	43.24	−73.42	1.726	44.5	8.95	0.25	1	75
J61A	43.35	−72.55	1.99	30.5	1.64	1	1	206
J62A	43.23	−71.81	1.696	30.5	2.33	1	3	56
J63A	43.28	−71.08	1.726	29.5	0.75	3	2	69
K57A	42.73	−76.52	1.846	41.5	0.64	3	2	47
K58A	42.76	−75.65	1.804	46	8.08	0.25	3	59
K59A	42.78	−74.85	1.702	48	9.26	0.25	3	58
K60A	42.62	73.89	1.798	40	8.15	0.25	1	29
K61A	42.67	−73.27	1.774	43	1.05	2	1	65
K62A	42.67	−72.23	1.696	31.5	1.17	2	3	230
K63A	42.69	−71.53	1.684	30	0.79	3	1	71
KRSG	43.34	−71.85	1.69	31	0.79	3	3	26
KSCT	41.73	−73.48	1.996	28	3.26	0.5	1	317
KSPA	41.56	−75.77	1.714	37.5	2.28	1	3	307
L57A	42.00	−76.85	1.6	25	10.83	0.25	1	75
L58A	42.04	−75.85	1.768	46.5	4.23	0.5	3	69
L59A	42.19	−75.04	1.648	25	10.03	0.25	1	80
L59A	42.19	−75.04	1.93	40	1.75	1	2	330
L61A	42.19	−73.55	1.81	39.5	2.01	1	2	67
L61B	42.45	−72.68	1.726	31.5	0.75	3	3	272
L63A	41.86	−71.61	1.798	34	0.68	3	3	57
L64A	41.94	−70.84	1.726	29	0.75	3	3	188
LATQ	47.38	−72.78	1.726	37	2.24	1	3	117
LBNH	44.24	−71.93	1.816	37	1.99	1	2	420
LONY	44.62	−74.58	1.984	38	0.83	2	2	413
LUPA	40.60	−75.37	1.906	38	0.9	2	3	381
M61A	41.31	−73.77	1.666	38	4.88	0.5	1	62
M62A	41.44	−72.89	1.702	31.5	4.63	0.5	2	61
M63A	41.40	−72.05	1.714	32.5	0.76	3	3	273
M64A	41.55	−71.21	1.702	30.5	0.77	3	3	39
M65A	41.56	−70.65	1.678	30.5	0.8	3	3	60
MCVT	43.96	−72.99	1.744	35	4.37	0.5	1	380
MNTQ	45.50	−73.62	1.816	34	1	2	3	480
N62A	40.93	−73.47	1.732	32	4.44	0.5	3	278
NCB	43.97	−74.22	1.774	45.5	1.05	2	1	408
NPNY	41.75	−74.14	1.816	37.5	1	2	2	267
O59A	40.31	−76.19	1.99	34	1.64	1	1	35
O60A	40.32	−75.41	1.648	25	0.84	3	1	70
ODNJ	41.08	−74.61	1.762	41.5	1.07	2	3	242
ORIO	45.45	−75.51	1.762	39.5	0.71	3	3	282
OTT	45.39	−75.72	1.774	38.5	0.7	3	3	288
P59A	39.61	−76.43	1.708	40	9.18	0.25	3	63

(*Continued*)

Table 1. *Continued*.

Station	Latitude (deg)	Longitude (deg)	V_p/V_s	Thickness (km)	Moho transition (km)	Maximum frequency (Hz)	H-k quality	Number of EQs
P60A	39.81	−75.64	1.714	32	0.76	3	1	44
PAHR	41.02	−75.71	1.732	43.5	4.44	0.5	2	135
PANJ	40.38	−74.70	1.75	39.5	4.33	0.5	3	268
PAPL	41.30	−75.02	1.732	43	0.74	3	3	123
PKME	45.26	−69.29	1.69	34	0.79	3	3	1251
PQI	46.67	−68.01	1.798	33.5	2.04	1	3	177
PSBK	40.36	−75.97	1.774	44	1.05	2	2	70
PSSK	40.64	−76.16	1.708	37.5	4.59	0.5	2	156
PTNY	44.56	−74.95	1.834	38.5	1.95	1	3	207
QMHP	43.75	−70.01	1.708	28	0.77	3	3	42
QUA2	42.28	−72.35	1.696	30.5	0.78	3	3	265
SHLB	42.60	−72.75	1.828	28	3.93	0.5	1	38
SNPE	43.34	−72.08	1.684	32	0.79	3	3	43
TRY	42.73	−73.67	1.732	42.5	0.74	3	1	455
TUPA	40.17	−75.19	1.744	29.5	2.18	1	3	313
VT1	44.32	−72.75	1.87	33	1.87	1	1	242
WBO	45.00	−75.28	1.768	37.5	0.71	3	3	140
WCNY	43.98	−75.65	1.78	42	0.69	3	3	355
WILL	42.71	−73.21	1.762	44.5	2.13	1	2	60
WVL	44.56	−69.66	1.738	35.5	1.1	2	3	218

Crustal thickness H, V_p/V_s and V_s were calculated using the H-k stacking method assuming a crustal P-wave velocity of 6.5 km s^{-1}. The wavelength was calculated using the maximum frequency of the coherently observable Moho pulse in the receiver functions, along with the estimated V_s. The Moho thickness is then calculated using the wavelength and the V_p/V_s ratio, as described in the text. EQs, earthquakes.

duration of analysis window and p is the time–bandwidth product, i.e. 2.5. We use a 140 s analysis window to ensure reliable measurements to *c.* 28 s delay time, based on the relation of the analysis window duration divided by twice a fixed time–bandwidth product of 2.5.

To identify the portion of the RF signals that do not vary as a function of direction, we apply a harmonic decomposition approach (Shiomi and Park 2008; Bianchi *et al.* 2010; Park and Levin 2016). This technique applies a linear regression to model the harmonic behaviour of the Q and T component RFs as a function of direction (as expressed by the station to event azimuth or backazimuth). While harmonic decomposition or similar approaches are often applied with the explicit goal of identifying dipping and/or anisotropic interfaces at depth (e.g. Schulte-Pelkum and Mahan 2014; Ford *et al.* 2016; Olugboji and Park 2016; Luo *et al.* 2023*a*), in this study we are only focused on the portions of the Q component RF signal that do not vary with direction.

H-k stacking

To obtain constraints on the thickness and composition of the crust, we use our MTC-generated RFs to generate H-k stacks (Zhu and Kanamori 2000; Linkimer *et al.* 2010, Levin *et al.* 2017; Link *et al.* 2020); an example of this method is shown in Figure 2b. H-k stacking uses a grid-search approach to best fit estimated crustal thickness (H) and V_p/V_s (k) values from the observed P_s phases and multiples (P_pP_s and $P_pS_s + P_sP_s$) observed within the time-series data, according to the following equations:

$$H = \frac{t_{P_s}}{\sqrt{\left(\frac{1}{V_S^2 - p^2}\right)} - \sqrt{\frac{1}{V_p^2 - p^2}}}, \quad (1)$$

$$H = \frac{t_{P_pP_s}}{\sqrt{\left(\frac{1}{V_S^2 - p^2}\right)} + \sqrt{\frac{1}{V_p^2 - p^2}}}, \quad (2)$$

$$H = \frac{t_{P_pS_s+P_sP_s}}{2\sqrt{\left(\frac{1}{V_S^2 - p^2}\right)}}, \quad (3)$$

where H is layer thickness, t_{P_s} (equation (1)), $t_{P_pP_s}$ (equation (2)), and $t_{P_pS_s+P_sP_s}$ (equation (3)), represent the delay times of converted P-to-S phases and corresponding multiples, V_p and V_s are the P-wave and S-wave velocity, respectively, and p is the ray parameter. The characteristic polarity of the multiple phase is positive for P_pP_s, followed by a negative

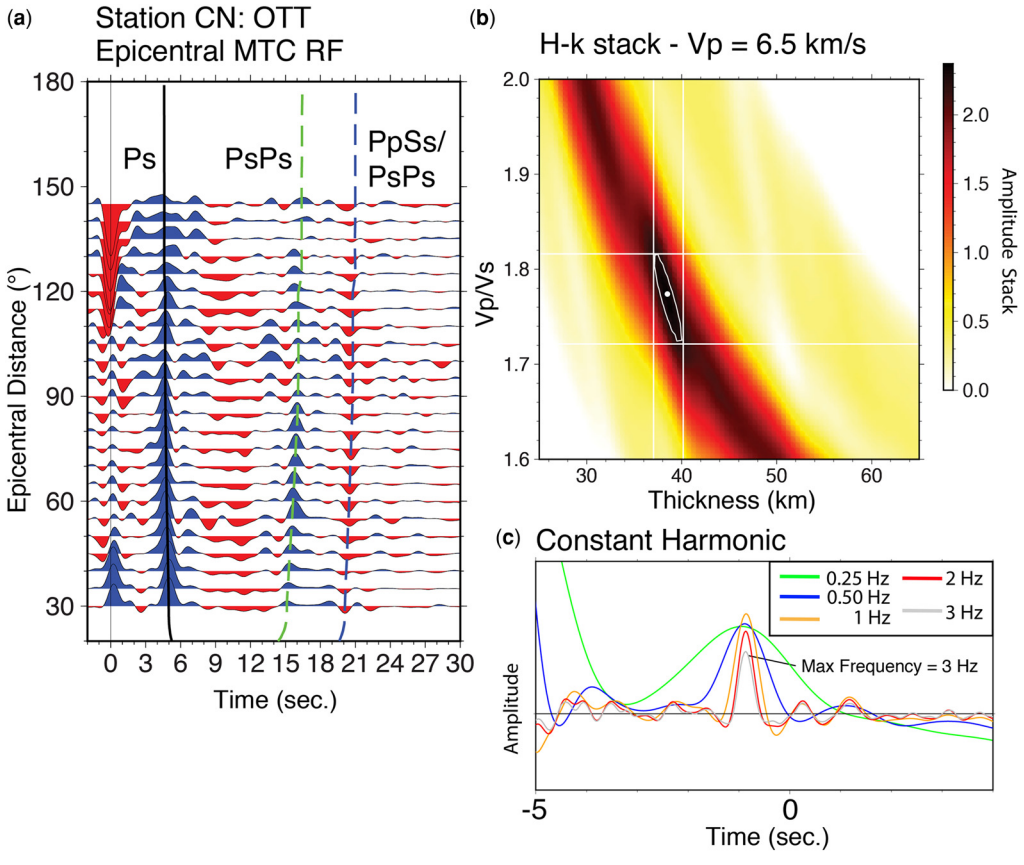

Fig. 2. Example results for each method used in the study from station CN: OTT. (**a**) Epicentral gather of multitaper receiver functions (RFs) (see Supplementary Table S1). Black line denotes the predicted timing of P_s converted phase, with the green and blue stippled lines showing the predicted timing of the multiples P_pP_s and $P_pS_s + P_sP_s$, respectively. RFs are binned in 5° increments with 50% overlap. (**b**) Results of omni-directional H-k stacking result. The white circle represents the maximum value for the stack, with the white contour being boundaries of 95% of the maximum. Horizontal and vertical white lines show the optimal values for both thickness and V_p/V_s. (**c**) Multifrequency, directionally invariant, constant harmonic multitaper RF results. Black arrow shows the highest chosen frequency at which a coherent P_s pulse is visible.

phase for $P_pS_s + P_sP_s$, with the time-delay between phases being controlled by the crustal thickness and V_p/V_s ratio.

We use a typical uniform value of 6.5 km s^{-1} for V_p throughout the region, matching results and workflows from many previous studies (Tesauro *et al.* 2014; Levin *et al.* 2017). To generate the stack, we use phase-determined weights of 70% for P_s, 20% for P_pP_s, and 10% for $P_pS_s + P_sP_s$, following the original implementation of the method (Zhu and Kanamori 2000). An assumption of the H-k stacking method requires a horizontal, homogenous impedance boundary to properly predict the timing of the P_s phase and multiples. This means that any directionally dependent P_s phase delay times related to complicated crustal structure or anisotropy will adversely affect the results (e.g. Linkimer *et al.* 2010; Link *et al.* 2020). We constrain the grid search to crustal thickness values of 25–65 km and V_p/V_s ratios of 1.6–2.0. These values for V_p/V_s encompass a reasonable range for crustal rocks and are based on previous laboratory studies (Christensen 1996, 2004). Because we do observe directional variability in the RF signal at many sites in our study, we computed directionally dependent RFs and found that the H-k stacking results at many stations depend on direction. Because of this, we chose to include data from all directions into our H-k stacking estimates; this has the effect of averaging directional dependence, although at the cost of increasing the uncertainty of our H-k estimates for sites with particularly complicated crust.

Moho sharpness estimates

The RF technique (Ammon 1991) focuses on S-waves generated by mode conversion of P-waves at interfaces with impedance contrasts. The pulse shape of the converted P_s wave allows the visual identification of coherent signals, which can be used to estimate the vertical extent of the impedance transition. Levin *et al.* (2016) modelled the frequency-dependent behaviour of P_s conversions at interfaces and found that boundaries with a vertically instantaneous impedance change (that is, an infinitely sharp interface) produced a progressively 'sharper' pulse of decreasing width with higher frequency. In contrast, a gradual vertical gradient in impedance, that is an interface with increasing impedance in finite step-wise intervals, produced decreasing pulse widths only up to a certain frequency limit. A complex crust–mantle transition resulted in a set of complicated but distinct pulses. Levin *et al.* (2016) used these insights to develop a method of estimating the thickness of the Moho boundary based on the frequency-dependent behaviour of RF traces, a strategy we follow here.

To make estimates of the Moho transition thickness, we visually inspect the RFs at each station and choose the highest maximum frequency (0.25, 0.5, 1, 2 or 3 Hz) at which a coherent Moho P_s pulse is observed. Frequency limits are based on previous work (Levin *et al.* 2016) and represent the higher end of resolvable teleseismic signals. We then calculate the relevant wavelength, assuming a P-wave velocity of 6.5 km s^{-1} and the best-fitting V_p/V_s ratio from our H-k stacking, from which we estimate the thickness of the transition between the crust and mantle. To identify the highest visible frequency, we use the constant component from our MTC RF harmonic decomposition estimates, which represents the directionally invariant portion of the P-SV signal (Fig. 2c). By isolating the directionally invariant portion of the signal, we can avoid complex, directionally variant noise. To focus on the Moho signal, we migrate all data to a depth of 50 km (so a time of 0 s corresponds to a depth of 50 km; see Fig. 2c), such that all Moho conversions arrive before $t = 0$. The velocity models used for time-to-depth conversion for each station were adapted from the IRIS EARS database (IRIS, DMC 2010; Trabant *et al.* 2012) and Li *et al.* (2021). After identifying the highest frequency at which the Moho pulse could be clearly identified, we calculated the Moho transition thickness using:

$$M = \frac{\lambda}{4}\left(\frac{\alpha}{\alpha - 1}\right), \quad (4)$$

where $\alpha = (V_p/V_s)$ and λ is the wavelength.

Assessing uncertainty

In addition to estimating crustal thickness and V_p/V_s, we also calculate 95% confidence intervals for H-k stacking results, as shown as white contours in Figure 2b. These values are obtained when a thickness and V_p/V_s pair has energy greater than 95% of the rest of the stack. The uncertainty for Moho sharpness was calculated by these maximum and minimum V_p/V_s estimates using equation (4). Uncertainties for crustal thickness, V_p/V_s and Moho sharpness measurements are reported in Table 1. Furthermore, we assign each of our measurements a quality rating; the highest quality measurements (quality 3) are described by a small and well-defined 95% confidence interval constrained by clear P_s multiple amplitude energy on epicentral RFs. Stations that have lower amplitude multiples in epicentral RF plots, or that form extended bands of 95% confidence intervals, are denoted as medium quality (quality 2). The poorest, least reliable measurements (quality 1) are those that have no observable epicentral RF multiples and have either a very large 95% confidence interval or multiple confidence intervals.

Results

Regional overview

We present our results in Table 1 and in map view in Figures 3–5, which show crustal thickness, V_p/V_s ratio and Moho thickness, respectively. We also select three transects along which we show cross-sections in Figures 6–8; two of these are along the dense SEISConn and NEST lines, while one is located further to the north (transect locations are shown in Fig. 3). A list of our results is shown in Table 1 and all maximum and minimum values are shown in supplemental table 1; supplementary Figure S1 compares all station results as scatter plots and histograms, highlighting more variability in results of stations with lower crustal thickness. Supplementary Figures 2S–132 show epicentral distance stacks of Q component RFs, H-k stacking results and multifrequency RF measurements (as in Fig. 2) for every station in our dataset.

Our results identify a striking first-order difference in crustal properties between Laurentian and Appalachian terranes, particularly when it comes to crustal thickness. The average values for all Laurentian stations in the Grenville belt are crustal thickness = 38 km (SD ± 5.8), $V_p/V_s = 1.77$ (SD ± 0.08) and Moho transition thickness = 3 km (SD ± 1.3). For Appalachian stations, average values are crustal thickness = 33 km (SD ± 4.8 km), $V_p/V_s = 1.75$ (SD ± 0.07) and Moho transition thickness = 2 km (SD ± 1.8 km). When we use only the better-

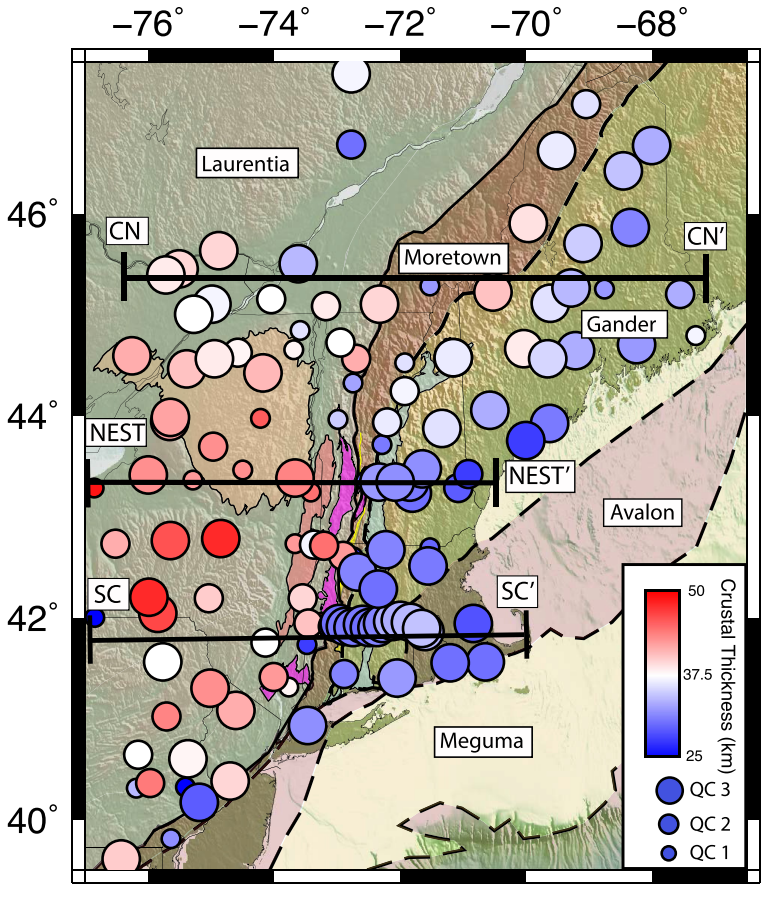

Fig. 3. Map of estimated crustal thickness throughout New England and surrounding region. Coloured circles show positions of seismic stations, with colour representing crustal thickness estimates (red = thicker; blue = thinner). Locations of transects SC–SC′, NEST–NEST′, and CN–CN′ are shown with lines. Tectonic unit boundaries and topography are as in Figure 1; circle size is representative of H-k stacking measurement quality, with largest circles having the highest quality (QC = 3), medium circles having moderate quality (QC = 2) and the smallest circles (QC = 1) being the least reliable. The QC values are described in the section 'Assessing uncertainty'. Stations are within 75 km of either side of the transect.

constrained H-k stacking estimates (QC values of 2 or 3 in Table 1), we find average values for Laurentian crustal thickness of 39 km (SD ± 3.3 km), 1.77 V_p/V_s (SD ± 0.058) and Moho transition thickness = 2.46 km (SD ± 2.48 km). For Appalachian stations, the crustal thickness is 33 km (SD ± 3.6 km), V_p/V_s = 1.74 (SD ± 0.06) and Moho transition thickness = 2 km (SD ± 2.05 km).

Crustal thickness

In agreement with previous studies (e.g. Li *et al.* 2018, 2020; Luo *et al.* 2021, 2023*b*), our results show a first-order difference between the relatively thick crust of Laurentia and the relatively thinner crust of the Appalachian terranes (Fig. 3). This lateral contrast is particularly pronounced from Connecticut north through central Vermont (41.94°, −73.18° to 43.29°, −73.01); in these regions, the transition from thicker crust in the west to thinner crust in the east coincides closely with the location of the Laurentian–Moretown suture. The west to east change in crustal thickness is most pronounced in southern New England; in contrast, northern New England stations do not exhibit a clear step-like change. Station CS02 of the temporary SEISConn experiment (network XP) has the thickest estimated crust, at 49.5 km (maximum thickness of 51.5 km and minimum thickness of 30 km). It is worth noting, however, that the constraint on crustal thickness and V_p/V_s at this site is particularly poor, probably owing to lateral complexity of the Laurentian–Appalachian

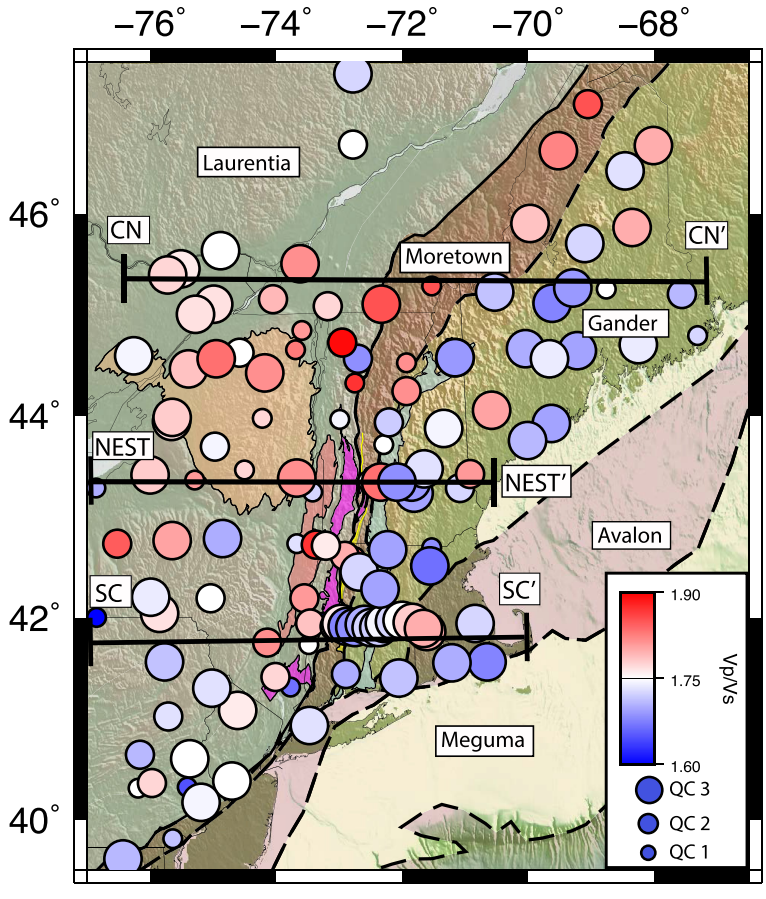

Fig. 4. Map of estimated V_p/V_s throughout New England and surrounding region. Coloured circles show positions of seismic stations, with colour representing V_p/V_s estimates (red = higher V_p/V_s; blue = lower V_p/V_s). Other plotting conventions are as in Figure 3.

suture directly beneath the station (Luo *et al.* 2021). The long-running (10+ years) permanent station US-BINY, located in Binghamton NY, has the second-thickest estimated crust at 48 km (maximum thickness of 49.5 km and minimum thickness 46 km), with a V_p/V_s estimate of 1.73 (maximum V_p/V_s of 1.78 km and minimum V_p/V_s of 1.702). The Appalachian terranes uniformly exhibit crustal thickness values less than 40 km, with almost all stations having a value between 28 and 35 km.

V_p/V_s

The map of V_p/V_s estimates from H-k stacking (Fig. 4) does not show regional variability as clearly as the crustal thickness map (Fig. 3); however, we do note some interesting patterns. We identify a region of systematically lower V_p/V_s within southern New England (Connecticut, Massachusetts, and Rhode Island, possibly extending north through southern New Hampshire). Furthermore, we observe a region with generally higher V_p/V_s near the Adirondack Mountains, extending east into northern Vermont and southern Canada. The average V_p/V_s for the entire study region based on our measurements is 1.75 (SD $\pm$ 0.077); however, this average is probably biased, as many H-k measurements are poorly constrained, particularly at temporary stations. We note that the H-k stacking methodology generally fails for stations directly over the suture between Laurentia and Appalachian terranes; this is probably a consequence of lateral heterogeneity at depth (associated with the transition from thick to thin crust).

Moho sharpness

Our Moho thickness results (Fig. 5) are more geographically variable than our crustal thickness and V_p/V_s estimates, although a few first-order patterns do emerge. In most areas of our study region, the

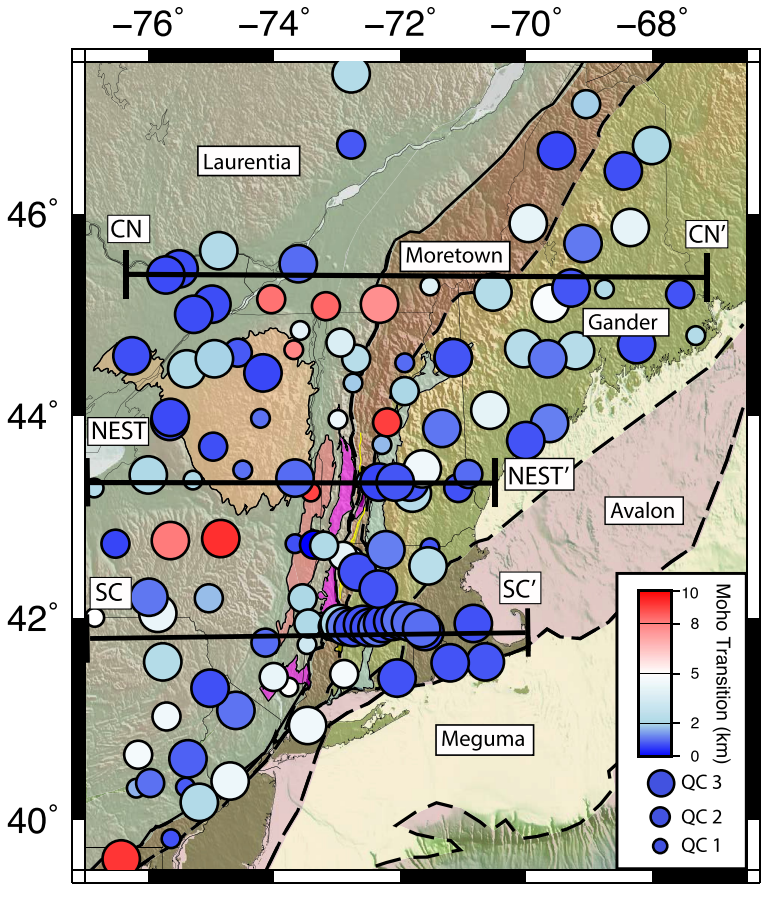

Fig. 5. Map of estimated Moho transition thickness throughout New England and surrounding region. Coloured circles show positions of seismic stations, with colour representing V_p/V_s estimates (red = higher V_p/V_s; blue = lower V_p/V_s). Other plotting conventions are as in Figure 3.

Moho is sharp; 44 out of 133 stations yielded a sharpness estimate of less than 1 km, with 101 out of 133 stations having a sharpness of less than 4 km. It is notable that all stations exhibiting Moho thickness values greater than 6 km lie either on Laurentia, close to the Laurentian–Moretown suture, or surrounding the Adirondack Mountains. A geographical trend can be seen most clearly along the dense SEISConn line, which displays systematically more gradational Moho transitions near the suture and uniformly sharp Moho interfaces beneath the accreted Appalachian terranes (discussed in detail below).

Results along selected transects

The SEISConn transect

The deployment of densely spaced seismic stations offers clear advantages over relying on more sparsely spaced arrays, as dense deployments afford the opportunity to probe structure on the length scales that are relevant to geological structures (Fig. 1b). Along transect SC–SC′, which aligns with the SEISConn temporary seismic experiment crossing the Laurentia–Moretown boundary in southern New England (Fig. 6), small-scale geographical variations in crustal properties are remarkably clear. To the west of the suture, we observe thick, if somewhat variable, crust, with Moho depths ranging from 37 to 48.5 km. Reliable V_p/V_s ratio measurements for these stations vary from *c.* 1.71 to 1.77. The Moho thickness varies significantly within the westernmost stations, with some stations showing sharp Moho but many stations showing Moho thickness values between *c.* 2 and 5 km, particularly stations located just to the west of the suture.

To the east of the suture, we see a pronounced transition in the character of crustal structure in all

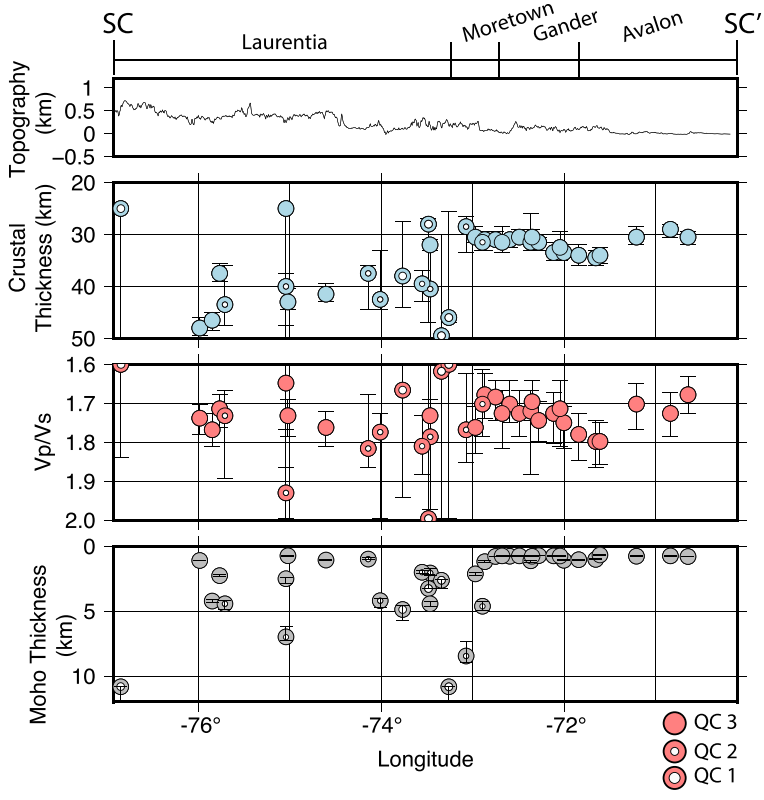

Fig. 6. Transect through southern New England along the SEISConn line (see transect location in Fig. 3). (**a**) Results for H-k thickness estimates as blue circles. Poorly constrained measurements are marked by a white circle inside the blue circle, with larger white circles meaning more uncertainty. Bars above and below blue dots show the 95% confidence regions for the H-k stacking results. (**b**) Results for H-k V_p/V_s estimates as red circles; again, white circles indicate uncertain estimates. Bars show 95% confidence regions for the H-k stacking results. (**c**) Estimates of Moho transition thickness. Names of locations and surficial boundaries are shown at the top of the profile for ease of comparison with map-based results.

three of our indicators (Fig. 6). There is an abrupt change in crustal thickness, with thinner crust (and better-constrained crustal thickness estimates) to the east of the suture. This pattern is similar to that identified by Luo *et al.* (2021, 2022) using different methodologies (common conversion point RF stacking and scattered wavefield migration, respectively, compared with the H-k stacking we carry out here). We also document a clear variability in V_p/V_s between Laurentia and accreted Appalachian terranes (with Laurentian stations showing considerable scatter and slightly higher V_p/V_s values on average). Also, within the accreted Appalachian terranes the V_p/V_s increases smoothly to the east across SEISConn, from 1.68 (maximum V_p/V_s of 1.73 and minimum V_p/V_s of 1.62) at station CS06 to 1.8 (maximum V_p/V_s of 1.86 and minimum V_p/V_s of 1.74) at station CS15. Differences in Moho thickness characteristics are also clearly visible between Laurentia and Appalachian terranes across the SEISConn line; we observe variable Moho thickness values for Laurentian stations, with many stations showing Moho thicknesses between *c.* 2 and 5 km. However, Appalachian terrane stations consistently show a very sharp Moho, with estimates of Moho thickness uniformly less than 1 km.

The NEST transect

The transect NEST–NEST′ (Fig. 7) encompasses the southern Adirondack Mountains and the Laurentian–Moretown boundary. This transect was chosen to overlie the closely spaced temporary seismic installations of the northern line of the ongoing NEST experiment, which features dense (*c.* 15–20 km) station spacing across eastern Vermont and New Hampshire. Results along this transect are somewhat similar to the transect SC–SC′ in southern New England in terms of

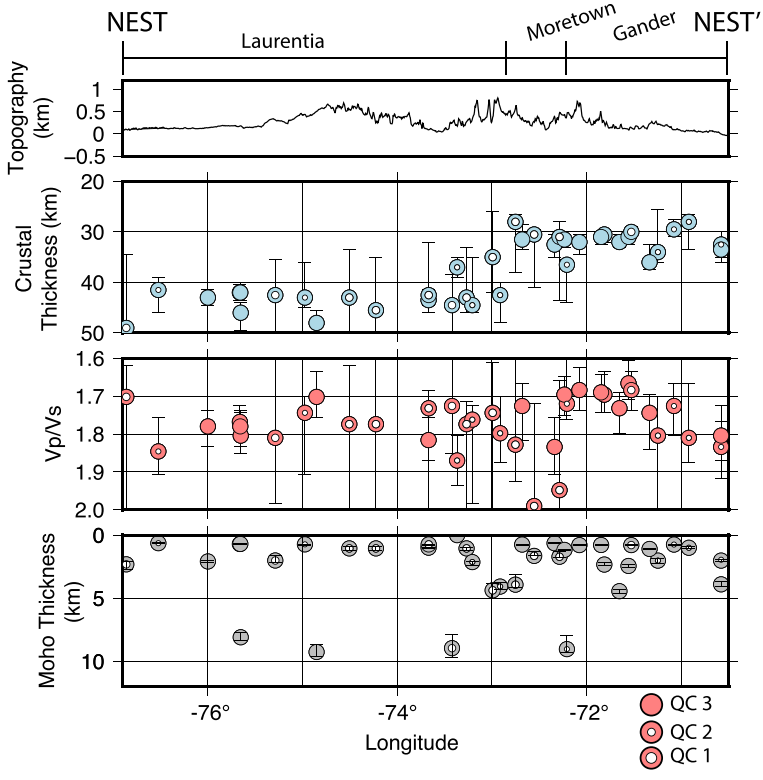

Fig. 7. Transect through New England along the NEST line (see transect location in Fig. 3). Plotting conventions are as in Figure 6.

crustal thickness, with values greater than 40 km at all stations to the west of the suture. Estimates of V_p/V_s measurements for Laurentian stations are scattered, but reliable sites J57A and WCNY show a value of 1.78 (maximum V_p/V_s of 1.83 and minimum V_p/V_s of 1.74). Moho thickness values for stations on Laurentia are generally small, with most values near *c.* 1 km and all less than *c.* 2 km. This pattern contrasts with the Laurentian crust to the south along the SC–SC′ line (Fig. 6).

East of the Laurentia–Moretown boundary, crustal thickness values decrease, although interestingly, the transition from thicker to thinner crust lies closer to the Moretown–Ganderia terrane boundary than the Laurentia–Moretown suture (Fig. 7). To the east, crustal thickness estimates are almost uniformly between 30 and 35 km, with the thickest crust (37 km; maximum thickness 39 km and minimum thickness 30 km) lying beneath station LBNH. The V_p/V_s values to the east of the Laurentia–Moretown suture have a similar pattern to that observed beneath transect SC–SC′ (Fig. 6), with a gradual increase in V_p/V_s going from west to east, ranging from *c.* 1.68 (maximum V_p/V_s of 1.74 and minimum V_p/V_s of 1.62) at station SNPE, to *c.* 1.80 at station I63A (maximum V_p/V_s of 1.87 and minimum V_p/V_s of 1.73). The Moho thickness beneath this transect is variable and shows significant geographical scatter (Fig. 7). The few stations with Moho thickness estimates greater than *c.* 2 km along this transect are all found on Appalachian terrane crust, a pattern that is distinctly different than that found to the south (Fig. 6).

The northern transect

The northern transect CN–CN′ (Fig. 8) shows significantly less lateral variation than do the two transects to the south. While there is a general decrease in crustal thickness from the west end of the transect to the east, the transition to thinner crust is gradual and the contrast between Laurentian crust (*c.* 40 km thick at the west end) and Appalachian crust (*c.* 35 km thick at the east end) is less pronounced. V_p/V_s values show only a modest trend, with the average of reliable H-k stacks at Laurentia stations near 1.77 (SD $\pm$ 0.058) and the average for Appalachian stations near 1.74 (SD $\pm$ 0.06). There is no pronounced difference between Laurentia and accreted Appalachian terranes in terms of Moho thickness, although

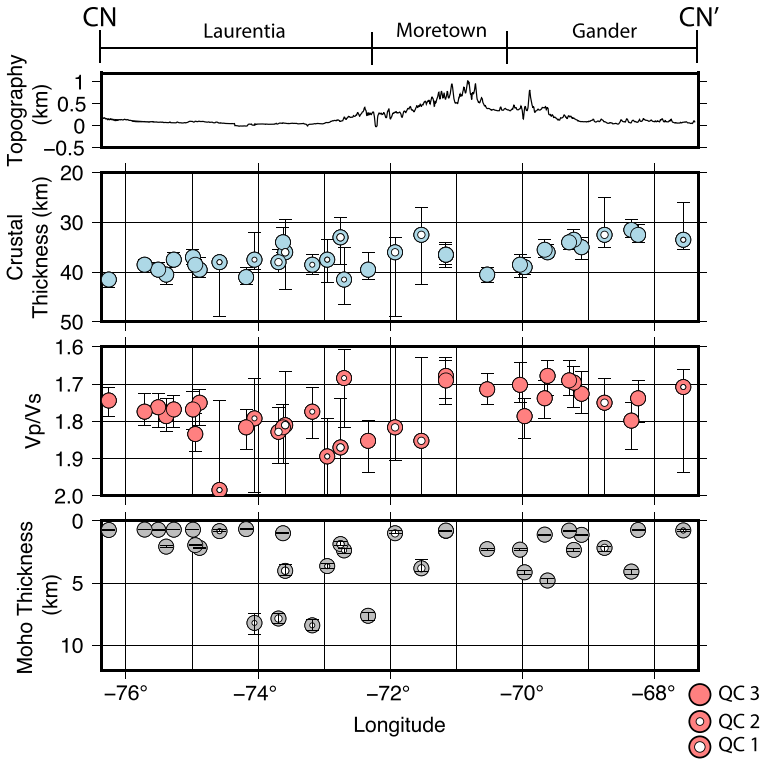

Fig. 8. Transect through northern New England (see transect location in Fig. 3). Plotting conventions are as in Figure 6.

stations at the extreme western end of the transect show sharper Moho than the rest of the transect, where Moho thickness values are scattered.

Summary of key observations

(1) We find the crust of the Grenville belt of Laurentia to be systematically thicker than the crust of accreted Appalachian terranes throughout New England, which is in good agreement with previous studies (e.g. Li *et al.* 2018, 2020). Furthermore, the nature of the transition from thick to thinner crust varies by latitude, with the southern and central transects showing a more pronounced and sharper change than the northern transect, also in accord with Li *et al.* (2018, 2020). The lateral change is particularly abrupt beneath the SEISConn line (Fig. 6). Notably, although there is a first-order difference between Laurentia and accreted Appalachian terranes, we do not generally see clear transitions in crustal thickness across the boundaries of individual Appalachian terranes (e.g. Moretown–Ganderia or Ganderia–Avalonia).

(2) The ratio of compressional and shear wave speeds (V_p/V_s) at stations for which we obtained reliable estimates lies within the range of 1.65–1.9. There is only a very slight difference between the average V_p/V_s for Laurentia v. Appalachian terranes (1.77 v. 1.74 for the best-constrained stations). The area around the Adirondack Mountains and the northern Moretown Terrane has relatively high (*c.* 1.9) V_p/V_s. We document systematic variation in V_p/V_s along the SEISConn transect, with a general increase from west to east.

(3) Estimates of Moho thickness exhibit a large amount of geographical scatter. All stations with Moho thickness estimate greater than 6 km are located on Laurentia or close to the Laurentian–Moretown suture. Southeastern New England exhibits particularly sharp Moho, with clear variability along the SEISConn line (more diffuse Moho to the west and sharper Moho to the east).

(4) Altogether, our maps and transects suggest a few regions with distinctive crustal properties. Southern New England (Connecticut, Rhode Island and southeastern Massachusetts)

exhibits the thinnest crust, the lowest V_p/V_s values, and has a consistently sharp (<1 km) Moho transition. Another region in the north of our study area (northern New York, Vermont and New Hampshire and southeastern Canada) also shows some distinctive characteristics. Here, the crust gradually thins from the west (Adirondacks) to the east. V_p/V_s values are generally high in this region, with lower V_p/V_s values to the east. Although Moho thickness values are scattered within the region, they are generally higher than elsewhere in our study area, with several stations showing relatively diffuse Moho transitions.

Discussion

Comparison with previous studies

In this study, we produce densified regional measurements of multitaper spectral correlated receiver function estimates (Park and Levin 2000), taking advantage of the H-k stacking methodology of Zhu and Kanamori, (2000) to constrain crustal thickness and V_p/V_s. Additionally, we present the first estimates of the crust–mantle transition thickness beneath New England. The results of our H-k stacking investigation and measurements of Moho thickness have produced several observations similar to findings from previous work. The Grenville belt of Laurentia and accreted Appalachian terranes are distinct in terms of crustal thickness (Musacchio *et al.* 1997; Li *et al.* 2018, 2020; Luo *et al.* 2021, 2022, 2023*a*, *b*; Masis *et al.*, 2024). However, the lateral transition between thinner crust of Appalachian terranes and thicker crust of the Grenville belt changes from southern to northern New England; we observe a steep gradient to the south and a gradual change in thickness to the north. The V_p/V_s measurements largely match previous work (e.g. Benoit *et al.* 2014; Levin *et al.* 2017); however, densification using temporary seismic deployments highlights the lithological uniqueness of the Appalachian southern New England crust in Connecticut, Massachusetts and Rhode Island. By complementing our H-k stacking estimates with frequency-dependent RF measurements of the crust–mantle transition, we note the uniquely sharp transition from crust to mantle rocks also in southern New England as discussed below. This sharp transition is interpreted to be an inherited feature of Acadian terrane accretion followed by subsequent orogenic collapse driven by mid-crustal flow described by Hillenbrand and Williams (2021) and Hillenbrand *et al.* (2021, 2023).

To the north of our study region, H-k stacking and Moho thickness investigations were conducted from northern Maine into Canada, crossing the Archean Superior craton, Proterozoic Grenville Province and Paleozoic Appalachian terranes, by Levin *et al.* (2017). They found that the Superior craton has thin crust (*c.* 35 km), generally low V_p/V_s and a sharper Moho transition. The Grenville Province has more variation in crustal thickness (averaging *c.* 40 km), with V_p/V_s generally larger than that of the Superior craton, with a sharp Moho transition. The Appalachians were reported to have the most variability of all the terranes, with variable thickness (*c.* 30–41 km), widely varying V_p/V_s, and Moho transition thickness up to *c.* 4.5 km. In general most stations examined both in our study and by Levin *et al.* (2017) have very similar H-k stacking results and modest differences in Moho sharpness estimates, with any discrepancies probably due to differences in data processing procedures and availability. For example, for station PKME, Levin *et al.* (2017) identified a crustal thickness = 34 km, $V_p/V_s = 1.684$, Moho transition = 7.5 km, whereas we find crustal thickness = 34 km (35 km maximum and 33 km minimum), $V_p/V_s = 1.69$ (maximum V_p/V_s of 1.732 and minimum V_p/V_s of 1.636) and Moho transition = 0.79 km (maximum transition of 0.82 km and minimum transition of 0.76 km) in our study.

An active-source study estimated the ratios of P and S wave velocities based on refraction data (the O-NYEX experiment) collected across Laurentia and the Appalachian terranes in the northern Adirondack Mountains, Vermont and New Hampshire (Musacchio *et al.* 1997). They found clear evidence for an eastward-dipping interface, corresponding to the Laurentia–Appalachian suture, extending *c.* 100 km to the east of the Champlain thrust belt. Furthermore, they found an average V_p/V_s of 1.81 for Laurentia and 1.73 for Appalachian terranes, similar to our results of 1.77 (SD $\pm$ 0.058) for Laurentia and 1.74 (SD $\pm$ 0.06) for the Appalachian terranes. Benoit *et al.* (2014) produced RF H-k stacks to investigate the Laurentia and the Proterozoic Scranton Rift in central Pennsylvania and New York. We obtained similar estimates of crustal thickness, e.g. 45 km for US: BINY and 48 km (maximum thickness of 49.5 km and minimum thickness of 46 km) in this study. However, in comparison our V_p/V_s estimates varied slightly, e.g. 1.85 at US: BINY and 1.738 (maximum V_p/V_s of 1.78 km and minimum V_p/V_s of 1.702) in this study, probably owing to differing data and the methods applied.

Recent work by Chai *et al.* (2022) also provides constraints on seismic velocities regionally beneath the eastern US, incorporating complementary datasets from surface waves, P_s receiver functions and Bouguer gravity (Fig. 9 background). Although gravity and surface waves allow for the resolution of smooth velocity variations laterally and with depth, RFs resolve discontinuous jumps in the velocity structure. Chai *et al.* (2022) applied several effective smoothing techniques in their work, primarily

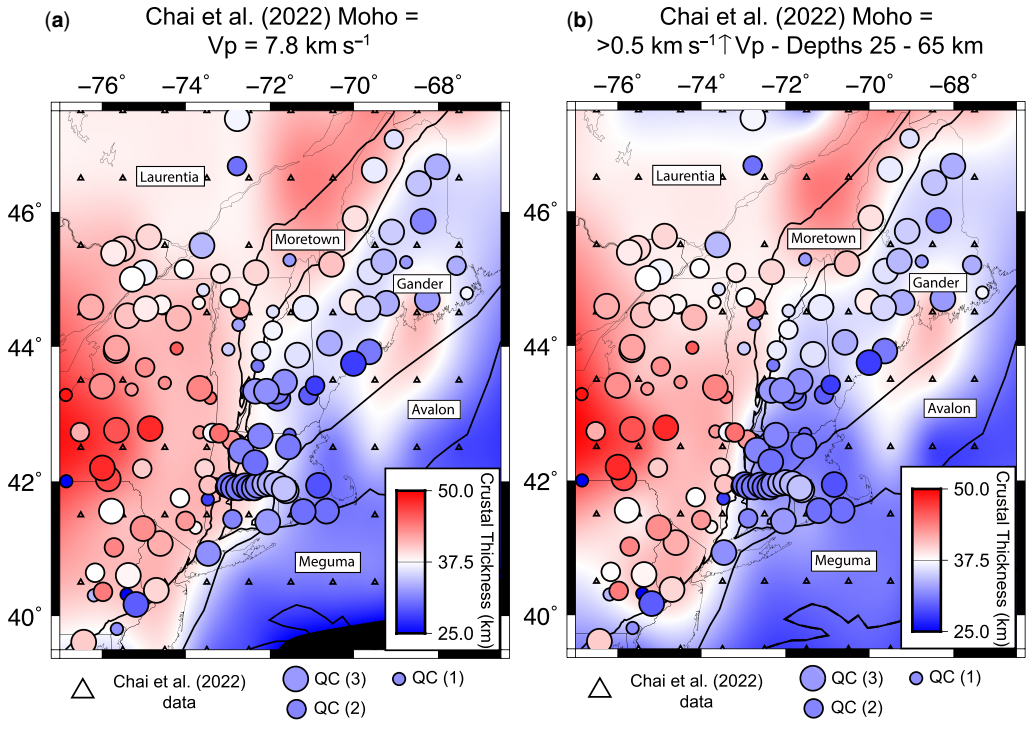

Fig. 9. Comparison between crustal thickness estimates from this study (circles) and those derived from the model of Chai *et al.* (2022). (**a**) Estimated the crustal thickness as the depth at which the model of Chai *et al.* (2022) reaches a P-wave velocity of 7.8 km s^{-1}; background colours indicate Chai *et al.* (2022) Moho depths, as indicated by the colourbar. (**b**) Estimated the crustal thickness as an increase in P-wave velocity of 0.5 km s^{-1} or more across a single depth grid node between 25 and 65 km depth in the Chai *et al.* (2022) model. In both panels, black lines are boundaries of Appalachian terranes. The circle size corresponds to the quality of the H-k stacking estimates, as in Figure 3. Black triangles show the position of grid points in Chai *et al.* (2022). Gridded surface was generated using GMT (Wessel *et al.* 2013).

with the aim of equalizing the lateral sensitivity of the RF constraints with the surface wave dataset. Consequently, the RF amplitudes at individual stations were systematically downweighted in the inversion of Chai *et al.* (2022) where lateral variation occurs, meaning that velocity discontinuities are potentially under-estimated.

We compare our estimates for crustal thickness with those of Chai *et al.* (2022) in Figure 9. We use two different potential definitions for the Moho, as derived from their tomography model. The first, a definition used by these authors, is the depth at which a P-wave velocity of 7.8 km s^{-1} P-wave is reached (see Fig. 9a). We also use a second definition: the depth at which a jump in velocity with depth (across a single depth grid node) can be identified that is larger than *c.* 0.5 km s^{-1} between 25 and 65 km depth. We plot these Moho depth estimates data in Figure 9b; interestingly, this definition produces a notably closer match to our estimates than the definition used in Figure 9a in several regions. Specifically, our Moho depth estimates in southern New England are closer to those from the Chai *et al.* (2022) model. Additionally, the Moho depth estimates from the surface wave model in Figure 9b to the north of the NY–Canadian border beneath Laurentia, and along the boundary of the Laurentia and the Appalachian terranes, tend to match our H-k stacking crustal thickness estimates better. We suggest that using a definition of crustal thickness that relies on a depth gradient in seismic velocity, rather than a single defined value for uppermost mantle velocity, may generally provide a better comparison between RF-based studies of crustal thickness and those based on seismic tomography.

Because Chai *et al.* (2022) incorporated P_s RF constraints into their tomography model, significant differences in estimated crustal thickness between our two studies would be unexpected. Modest differences, however, are not surprising, given the lateral smoothing used by Chai *et al.* (2022) and variability in our respective approaches to computing RFs (e.g.

differences in data processing and stacking strategies).

Key interpretable features

Interpolated surfaces of crustal thickness (Fig. 10), V_p/V_s (Fig. 11) and Moho transition zone thickness (Fig. 12) were produced using an empirical Bayesian kriging technique (Krivoruchko 2012). Kriging formulas weight surrounding measured values to make predictions for unmeasured locations. The empirical Bayesian approach automates the most challenging aspects of building a valid kriging model through the creation of subsets of the data and assessing the uncertainty of the semivariogram used in kriging. To account for spatial uncertainty, prediction error maps are provided in Figures S133. The V_p/V_s interpolated map (Fig. 11) highlights the distinctively low (*c.* 1.73) V_p/V_s ratio of the Appalachian terrane crust in southern New England and Maine as compared with the surrounding region. In contrast, V_p/V_s ratios beneath Laurentia in northern New York, and the Appalachian terranes in Vermont and NW New Hampshire have notably higher values (1.79 and higher), particularly in Vermont and the northeastern Adirondack Mountains into Canada (*c.* 1.84). The crustal thickness interpolated map (Fig. 10) shows the clear dichotomy in crustal thickness between the accreted Appalachian terranes and Laurentia. Additionally, a region of distinctively thicker Laurentian crust within upstate New York is identified, with thickness exceeding 40 km at most stations south of the Adirondack Mountains. Our results for Moho transition tend to show less distinctive regional patterns; we observe mostly sharp Moho transitions in general, particularly in the eastern portions of the accreted terranes (<2 km). However, the Moho transition is

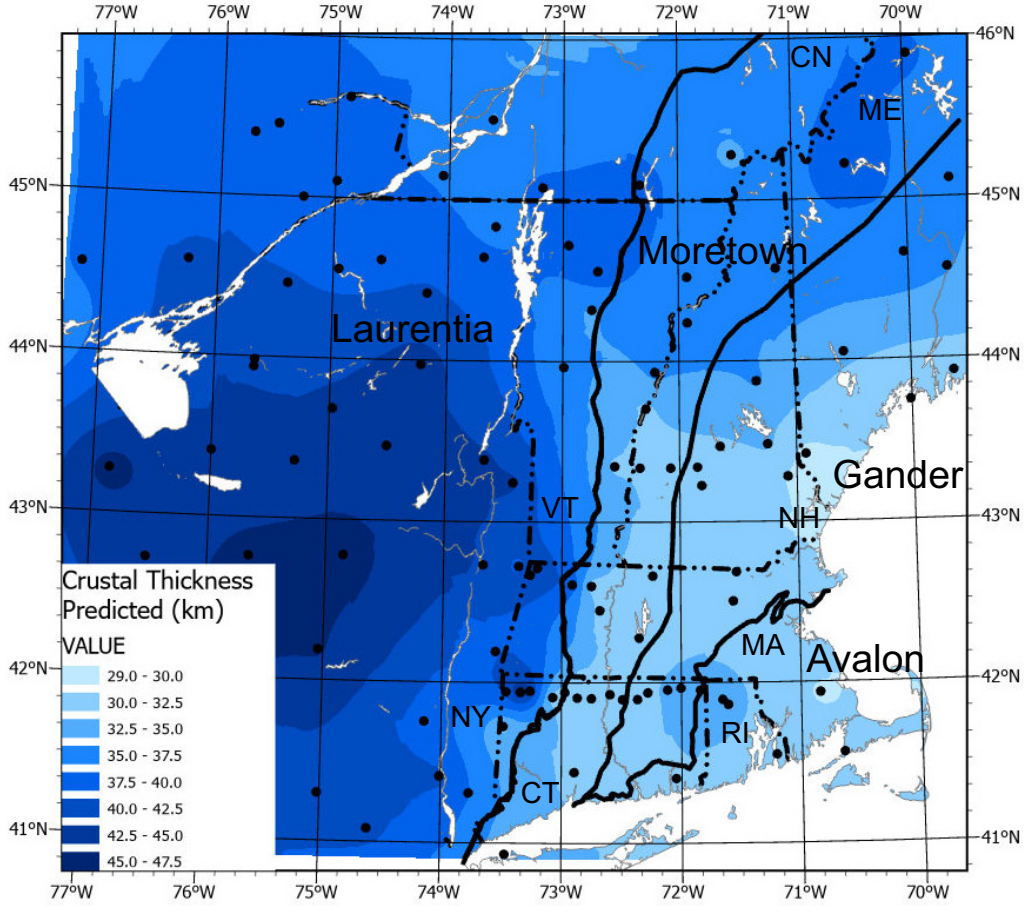

Fig. 10. Map of the northeastern US and southeastern Canada showing interpolated surface created using an empirical Bayesian kriging technique of crustal thickness using data from Table 1. Solid black lines show the suture between Laurentia and accreted Appalachian terranes (note that the boundary is not well constrained in Quebec).

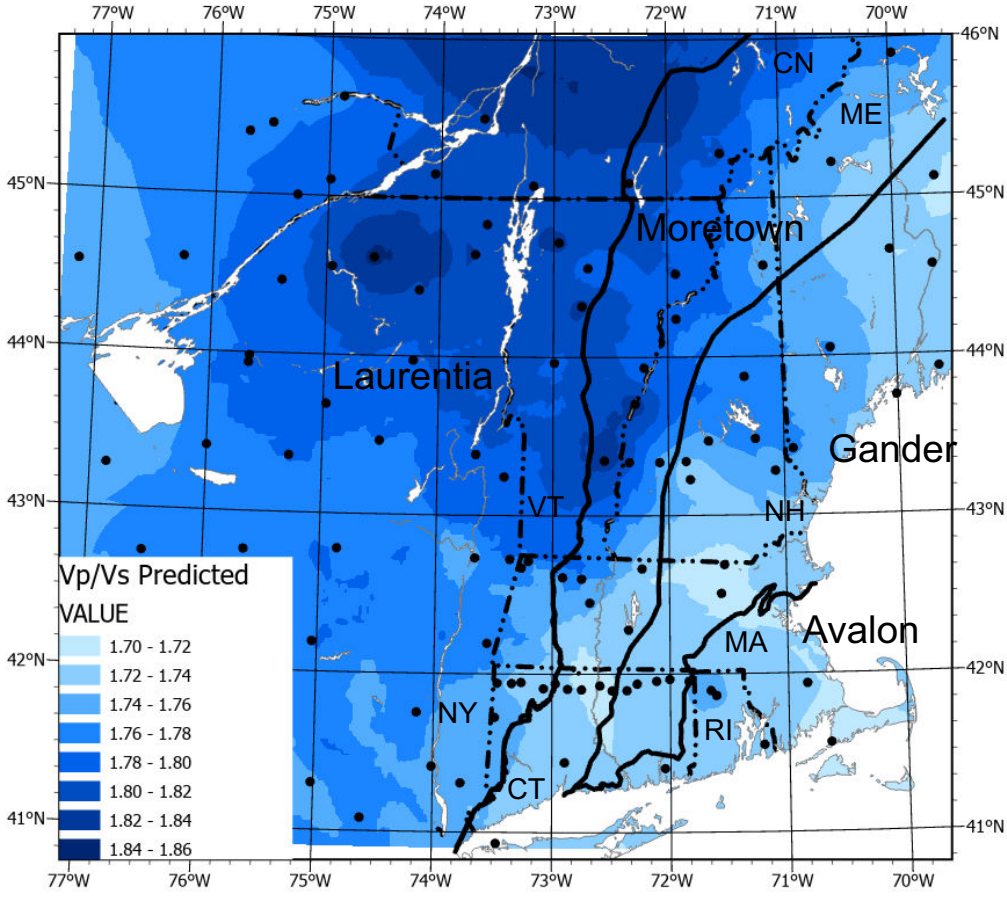

Fig. 11. Map of the northeastern US and southeastern Canada showing interpolated surface created using an empirical Bayesian kriging technique of average crustal V_p/V_s using data from Table 1. Solid black lines show the suture between Laurentia and accreted Appalachian terranes (note that the boundary is not well constrained in Quebec).

clearly more diffuse near the Laurentian–Appalachian suture throughout the entire region (>2 km).

Interestingly, there are a few geographic patterns that might have been expected that are not resolved in our study region. Specifically, we do not see any evidence for the trace of the *c.* 125–100 Ma Great Meteor Hotspot (33°N, 28°W) (e.g. Kinney *et al.* 2021) in our measurements of crustal properties, suggesting that hotspot passage did not result in widespread crustal modification or reworking (although such modification may potentially be locally identifiable on length scales smaller than our station spacing of *c.* 70 km). Additionally, we do not generally identify clear differences in crustal properties across the boundaries between individual Appalachian terranes, in contrast to the sharp contrast in some properties across the Laurentia–Moretown terrane suture.

A striking finding of this study is that southern New England stands out as a region of distinctive crustal properties within our study area (Figs 10–12). These distinctive properties include the presence of the Moho step across the Laurentian–Moretown terrane, a particularly sharp Moho transition beneath Appalachian terranes (and a clear transition from diffuse Moho beneath Laurentia to a sharper Moho beneath Appalachian terranes), with thin crust beneath the accreted Appalachian terranes, and low estimated V_p/V_s.

Geological and tectonic interpretations

Laurentian v. Appalachian crust

Differences in crustal thickness between Laurentia and the accreted Appalachian terranes have been

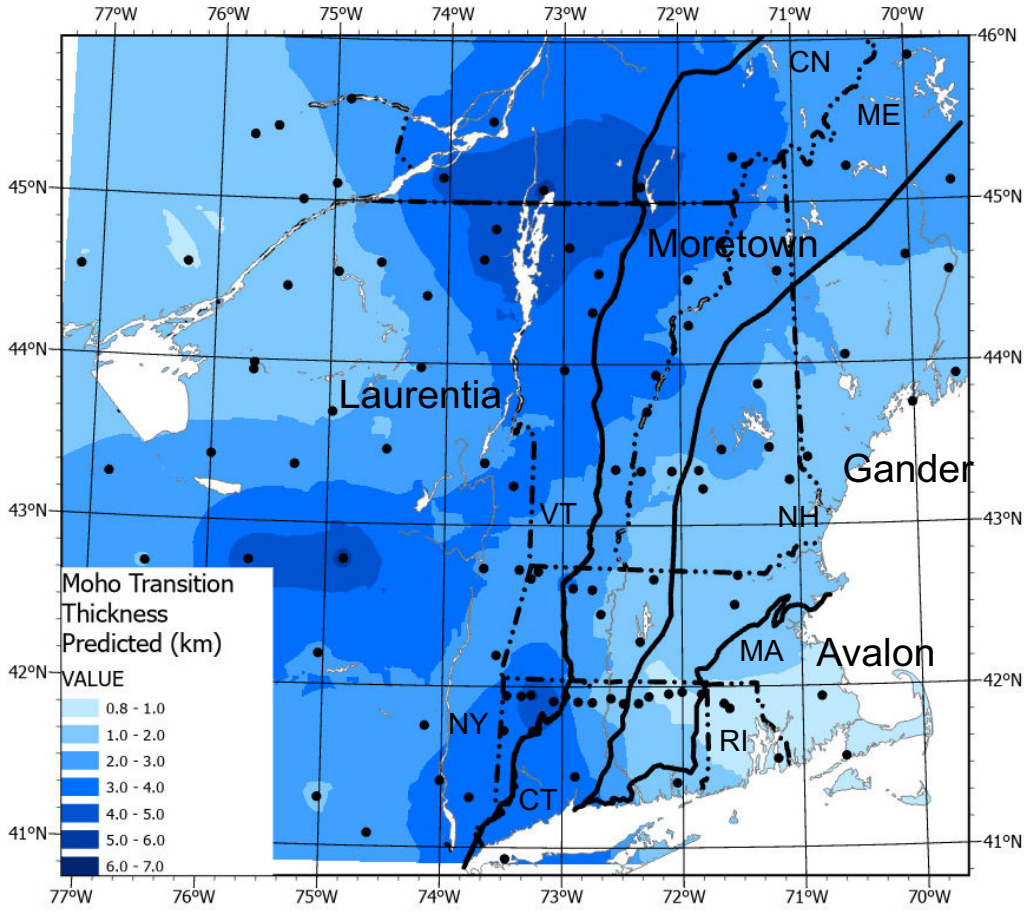

Fig. 12. Map of the northeastern US and southeastern Canada showing interpolated surface created using an empirical Bayesian kriging technique of Moho transition thickness using data from Table 1. Solid black lines show the suture between Laurentia and accreted Appalachian terranes (note that the boundary is not well constrained in Quebec).

observed in several large-scale seismic studies in the central and northern Appalachians (e.g. Shen and Ritzwoller 2016; Li *et al.* 2018, 2020). The Appalachian terranes are primarily composed of Gondwanan-derived, microcontinents with arcs that were built on them as they transited the Iapetus or Rheic oceans. They formed during the amalgamation of the supercontinent Rodinia (Hynes and Rivers 2010), and the rifted margin of Laurentia west of the suture with accreted Appalachian terranes forming during the Neoproterozoic break-up of Rodinia (e.g. McLelland *et al.* 2010, 2013). Laurentian crust may have been thickened by mafic magmatic underplating during Neoproterozoic rifting (Benoit *et al.* 2014; Yang and Gao 2018; Li *et al.* 2023). Globally, Proterozoic crust on average is thicker (*c.* 45 km) compared with average Archean or Phanerozoic crust (*c.* 35 km) and is generally thought to include a mafic basal layer (Durrheim and Mooney 1991; Holbrook *et al.* 1992; Christensen and Mooney 1995; Ganne *et al.* 2018; Cawood and Hawkesworth 2019). Thickening of the Laurentian crust owing to mafic underplating would also explain the difference in V_p/V_s that we observe in our study; a basal layer of mafic materials would be expected to increase the bulk average V_p/V_s of the crust.

Regionally, stations above the Laurentian–Appalachian suture systematically produce measurements with increased uncertainty (e.g. V_p/V_s ~1.6–1.9 convergence and broad crustal thickness ranges *c.* ±5 km). This complexity may be explained by dipping (and potentially sheared and thus anisotropic) contact between the Laurentian and Appalachian

crust. Given the underlying assumptions of the H-k stacking method (e.g. horizontal interfaces), this observation is not unexpected.

The unique southern New England crust

Based on EarthScope data, Li *et al.* (2018, 2020) showed that the crustal structure across the Appalachian terranes and Laurentia in southern New England was offset in a step-like pattern. The details of this crustal step were further delineated by the temporary seismic deployments SEISConn and NEST, which provided *c.* 15–20 km station spacing across the Appalachian–Laurentia suture in Connecticut, Massachusetts and Vermont (Long and Aragon 2020; Luo *et al.* 2021, 2022, 2023*a*; Goldhagen *et al.* 2022; Masis *et al.* 2024). Our work confirms previous findings that an abrupt step in crustal thickness is observed beneath southern New England (Connecticut and Massachusetts; Luo *et al.* 2021; Masis *et al.* 2024). In contrast, further to the south, the MAGIC temporary deployment in the Central Appalachians installed densely spaced seismic installations across the Laurentian–Appalachian suture and identified a more gradual change in crustal thickness from *c.* 55 km to *c.* 40 km over approximately 200 km (Evans *et al.* 2019; Long *et al.* 2019, 2020; Luo *et al.* 2023*a*). This gradient is comparable with the patterns that we document in northern New England, with changes in crustal thickness from *c.* 40 to *c.* 30 km across the Laurentian–Appalachian boundary. High uncertainties for measurements near the suture may be caused by deformation associated with orogenesis, with lower crustal modification probably producing a complicated crust–mantle boundary. The step-like change seems to be unique to southern New England, suggesting a distinct set of tectonic processes operating in this region in the geological past. Luo *et al.* (2021, 2023*b*) and Masis *et al.* (2024) have proposed a model in which compression and shortening during the Acadian orogeny reactivated previously existing east-dipping structures, producing overthrusting of rifted Laurentian crust and/or Moretown terrane crust to the west and forming a step-like feature with a doubled Moho signature.

A model that invokes significant compression and shortening associated with the Acadian orogeny was proposed by Hillenbrand *et al.* (2002, 2021, 2023). They proposed that the crust of southern New England experienced widespread thickening from 425 to 380 Ma and was an orogenic plateau from 380 to 330 Ma. They further proposed that the plateau collapsed at *c.* 330 Ma, via a combination of processes that may have included lower crustal delamination (Levin *et al.* 2000), deep crustal ductile flow and thinning (Hillenbrand *et al.* 2022), erosion and isostatic adjustment. Hillenbrand and co-workers attributed the sharp step in crustal thickness in southern New England to the reactivation of the Laurentia–Moretown suture as the plateau collapsed over tens of millions of years.

Our finding of a distinctive set of crustal properties for southern New England generally agree with the interpretations of Hillenbrand and others, Luo *et al.* (2021, 2023*b*) and Masis *et al.* (2024), who all invoked a distinctive set of tectonic processes operating in this region associated with the formation and collapse of the Acadian plateau. The systematically low V_p/V_s values (*c.* 1.73) that we document in the accreted Appalachian terranes of southern New England indicate a felsic (silica-rich) bulk crustal composition. This is similar to the measured bulk-crustal V_p/V_s of present-day orogenic plateaus such as the Tibetan Plateau, where V_p/V_s values range between 1.7 and 1.75 (Nábělek *et al.* 2009; Murodov *et al.* 2022), and the Bolivian Altiplano, with estimated V_p/V_s values of *c.* 1.6 (Zandt *et al.* 1994) to *c.* 1.73 (Swenson *et al.* 2000). The collapse of the Acadian Altiplano in southern New England may have altered the crustal composition via gravity-driven lithospheric loss or delamination of the lower crust, which may have accompanied crustal thinning during plateau collapse. It may be that widespread, uniform loss of (dense and probably mafic) lower crustal material during plateau collapse shaped the particularly sharp Moho that we observe beneath southern New England (Fig. 12). More generally, the formation and/or collapse of the Acadian Plateau may have led to the particularly thin crust and low V_p/V_s values we observe in this region today.

Limitations in observations

Our V_p/V_s estimates are less well constrained than our crustal thickness estimates, owing to the nature of the H-k stacking method. A small dip (*c.* 5°) to the Moho can delay or advance the arrival of multiples by as much as 2–3 s from different azimuths (e.g. Zhu and Kanamori 2000; Linkimer *et al.* 2010; Link *et al.* 2020). This effect can produce significantly distorted V_p/V_s estimates (e.g. Linkimer *et al.* 2010; Link *et al.* 2020). Our use of large datasets that include earthquakes arriving from a range of directions and distances may help to reduce the effect of crustal heterogeneity on our estimates. Our work has assumed a nominal value of 6.5 km s^{-1} P-wave velocity for the crust, which is comparable with the global average of 6.45 km s^{-1} for continental crust (Christensen and Mooney 1995). The influence of changing the background crustal P-wave velocity by 5% (6.5–6.2 km s^{-1}) would result in crustal thickness estimates differing by *c.* 2 km and V_p/V_s by *c.* 0.02 (Levin *et al.* 2017).

Factors affecting the V_p/V_s of the crust include fluid pore pressure, rock texture and composition.

Higher V_p/V_s ratios are associated with increased pore pressure, ray path geometries that are strongly aligned with the foliation or decreased SiO_2 content (Musacchio *et al.* 1997; Hughes *et al.* 1993; Kern and Tubia 1993). Distinguishing among these different factors can be difficult, particularly in tectonically complex regions. For example, we document particularly high V_p/V_s (*c.* 1.84 and greater) within our study area in the northern Adirondacks and central Vermont. Previous work has imaged a ramp-like crustal transition (known as the Grenville ramp) between Laurentian and Appalachian rocks (Musacchio *et al.* 1997). Although dipping boundaries can strongly affect the results of the H-k stacking methodology, northern Vermont does include widespread exposures of ultramafic rocks, which have intrinsically higher V_p/V_s. Economically relevant altered ultramafic rocks (Thetford) are present just to the north in Quebec (Whitehead *et al.* 2000; Tremblay and Castonguay 2002; Tremblay and Pinet 2016), with the Laurentian–Moretown suture being decorated with ultramafic tectonic lenses from Connecticut to Quebec (Ando *et al.* 1984; Stanley *et al.* 1984; Stanley and Ratcliffe 1985). It is important to note, however, that the region with the highest V_p/V_s ratios does overlie stacked altered rift-drift sediment packages in the shallow (<5 km) crust (Ando *et al.* 1984; Ratcliffe *et al.* 2011). Additionally, large ophiolite bodies are present in southern Quebec near the rifted Laurentian margin (e.g. De Souza *et al.* 2012) and they may be present further south in the subsurface. This may argue for particularly mafic crust in northern New England, although some caution is warranted in this interpretation because of the presence of dipping crustal structures.

Implications of the diffuse Moho near the Laurentian–Appalachian suture

The Moho transition thickness is commonly sharp (<2 km) in the New England Appalachians, except in the vicinity of the Laurentian–Appalachian suture, particularly immediately west of the suture. We observe more diffuse Moho transitions both in southern New England, in the vicinity of the Moho step, and in northern New England. As noted previously, this region experienced intense deformation in the early phases of Appalachian orogenesis, with the accretion of the Moretown terrane onto Laurentia beginning at *c.* 470 Ma (Karabinos *et al.* 2017). We speculate that the pattern of a diffuse Moho transition near the suture may have to do with the accretion of the Moretown terrane along the rifted margin of Laurentia and later reactivation of the east-dipping subduction zone during the Acadian orogeny (Luo *et al.* 2023*a*, *b*). The fact that most stations exhibiting gradational Moho are located near the Laurentian suture might also indicate a systematic structural origin. As such, a strongly dipping interface or underplating may produce an artificial diffuse Moho in the constant term of the receiver function harmonics used in our analysis. This possible effect will be further investigated in the future. We speculate that the pattern of a diffuse Moho transition near the suture may have to do with the accretion of the Moretown terrane along the rifted margin of Laurentia and later reactivation of the east-dipping subduction zone during the Acadian orogeny (Luo *et al.* 2023*a*, *b*).

Summary

In this study we present a comprehensive, uniformly processed set of estimates of crustal thickness, bulk crustal V_p/V_s, and Moho sharpness for the northeastern US and southeastern Canada. This region has been affected by a set of fundamental tectonic processes in the past, including orogenesis, continental rifting and potential post-rift modification by the Great Meteor Hotspot. We identify several first-order features of the crust in our study region, each providing insights into past tectonic processes. We find thick crust beneath Laurentia and thinner crust beneath the accreted Appalachian terranes, in agreement with previous studies. Specifically, for the stations with well-constrained H-k stacks (QC 2 and 3), Laurentia has an average crustal thickness of 39 km (SD $\pm$ 3.3 km), a V_p/V_s of 1.77 ($\pm$0.058) and a Moho transition thickness of 2.46 km ($\pm$2.48 km). For Appalachian stations, the average crustal thickness is 33 km ($\pm$3.6 km), V_p/V_s is 1.74 ($\pm$0.06) and the Moho transition thickness is 2 km ($\pm$2.05 km). We confirm the existence of a sharp, nearly step-like transition from thick Laurentian to thin Appalachian crust beneath southern New England and document a more gradual and subtle transition to the north. We identify particularly low V_p/V_s values in southern New England, with particularly high V_p/V_s in the Adirondacks, Vermont, and just to the north of these areas in Canada. While the Moho is generally sharp (with thickness less than 2 km) throughout most of our study area, there are a few exceptions; specifically, we document more diffuse Moho transitions near the Laurentian–Appalachian suture. The crust of southern New England is distinctive in several aspects, including the presence of the Moho step, particularly thin Appalachian terrane crust, a particularly sharp Moho beneath the Appalachian units and particularly low V_p/V_s values. These observations are generally consistent with a model of orogenic plateau formation during the Acadian orogeny (with subsequent plateau collapse) recently proposed by Hillenbrand *et al.* (2021, 2022, 2023). Notably, we do not observe regional variations in our estimated bulk crustal properties

that suggest widespread crustal alteration during either the break-up of Pangaea or the later passage of the Great Meteor Hotspot. We also observe a striking lack of differences in bulk crustal properties among individual accreted Appalachian terranes; whereas there is a first-order contrast between Laurentian and Appalachian terranes, individual accreted terranes do not exhibit clear distinctive signatures in bulk crustal properties.

Acknowledgements We thank participants in the NEST, SEISConn and GENESIS experiments for thorough and productive discussions on New England geology. We thank Dr Vadim Levin for his assistance with field work and discussions on New England tectonics, and his thoughts at the earliest stage of this project. Finally, we thank Shubham Agrawal, an anonymous reviewer, and the editor for constructive comments that helped to improve the paper.

Competing interests The authors declare that they have no known competing financial interests or personal relationships that could have appeared to influence the work reported in this paper.

Author contributions **JRB**: conceptualization (lead), data curation (lead), formal analysis (lead), investigation (lead), methodology (lead), writing – original draft (lead), writing – review & editing (lead); **MDL**: conceptualization (supporting), investigation (supporting), writing – review & editing (supporting); **FL**: methodology (supporting), writing – review & editing (supporting); **PK**: conceptualization (supporting), investigation (supporting), writing – review & editing (supporting); **LW**: investigation (supporting), writing – review & editing (supporting); **YL**: data curation (supporting), writing – review & editing (supporting); **KE**: data curation (supporting), writing – review & editing (supporting); **RM**: data curation (supporting), writing – review & editing (supporting); **YL**: data curation (supporting), writing – review & editing (supporting).

Funding The NEST experiment is supported by the National Science Foundation via grants to Yale University (EAR-2147536), Rutgers University (EAR-2147426), Williams College (EAR-2146804), and the University of Vermont (EAR-2147463). The SEISConn seismic experiment was supported by Yale University and the National Science Foundation under grants EAR-1150722 and EAR-1800923. We are grateful to the EarthScope Primary Instrument center (EPIC), formerly the IRIS PASSCAL Instrument Center, at New Mexico Tech for their support of the NEST deployment. EPIC and EarthScope Data Services are funded through the National Science Foundation's Seismological Facility for the Advancement of Geoscience (SAGE) Award under Cooperative Agreement (EAR-1724509).

Data availability All data are publicly available through the data archiving services provided by EarthScope Consortium Data Management center (https://ds.iris.edu/ds/nodes/dmc/). The specific networks that provided data for this study include: Canadian National Seismograph Network (CN), Global Seismograph Network (IU), Lamont–Doherty Cooperative Seismographic Network (LD), Central and Eastern US Network (N4), New England Seismic Network (NE), Pennsylvania State Seismic Network (PE), Portable Observatories for Lithospheric Analysis and Research Investigating Seismicity (PO), USArray Transportable Array (TA), United States National Seismic Network (US), Deep Structure of Three Continental Sutures in Eastern North America (X8), New England Seismic Network (7O) and Seismic Experiment for Imaging Structure beneath Connecticut (XP), and can individually searched at https://ds.iris.edu/mda/#pnetlist.

Figures 1–8 were produced using the Generic Mapping Tools GMT (Wessel *et al.* 2013). The maps in Figures 9 were produced using the Esri ArcPro. The receiver function time series analysis was conducted using the Recfunk21 series of software (https://github/com/RUseismology/Recfunk21).

References

Aiken, C.L. 2018. *Geochronologic Constraints on the Timing of Metamorphism and Exhumation of the Tillotson Peak Complex in Northern Vermont*. The University of Vermont and State Agricultural College.

Ammon, C.J. 1991. The isolation of receiver effects from teleseismic P waveforms. *Bulletin of the Seismological Society of America*, **81**, 2504–2510.

Ando, C.J. *et al*. 1984. Crustal profile of mountain belt: COCORP deep seismic reflection profiling in New England Appalachians and implications for architecture of convergent mountain chains. *AAPG Bulletin*, **68**, 819–837.

Bagherpur Mojaver, O. and Darbyshire, F. 2022. Crustal structure beneath the northern Appalachians and the eastern Grenville Province. *Journal of Geophysical Research: Solid Earth*, **127**, e2021JB023246, https://doi.org/10.1029/2021JB023246

Benoit, M.H., Ebinger, C. and Crampton, M. 2014. Orogenic bending around a rigid Proterozoic magmatic rift beneath the Central Appalachian Mountains. *Earth and Planetary Science Letters*, **402**, 197–208, https://doi.org/10.1016/j.epsl.2014.03.064

Bianchi, I. *et al*. 2010. Mapping seismic anisotropy using harmonic decomposition of receiver functions: an application to Northern Apennines, Italy. *Journal of Geophysical Research: Solid Earth*, **115**, https://doi.org/10.1029/2009JB007061

Cawood, P.A. and Hawkesworth, C.J. 2019. Continental crustal volume, thickness and area, and their geodynamic implications. *Gondwana Research*, **66**, 116–125, https://doi.org/10.1016/j.gr.2018.11.001

Cawood, P.A., McCausland, P.J. and Dunning, G.R. 2001. Opening Iapetus: constraints from the Laurentian margin in Newfoundland. *Geological Society of America Bulletin*, **113**, 443–453, https://doi.org/10.1130/0016-7606(2001)113<0443:OICFTL>2.0.CO;2

Chai, C., Ammon, C.J., Maceira, M. and Herrmann, R. 2022. Crust and upper mantle structure beneath the Eastern United States. *Geochemistry, Geophysics,*

Geosystems, **23**, e2021GC010233, https://doi.org/10.1029/2021GC010233

Chiarenzelli, J., Lupulescu, M., Cousens, B., Thern, E., Coffin, L. and Regan, S. 2010. Enriched Grenvillian lithospheric mantle as a consequence of long-lived subduction beneath Laurentia. *Geology*, **38**, 151–154, https://doi.org/10.1130/G30342.1

Christensen, N.I. 1996. Poisson's ratio and crustal seismology. *Journal of Geophysical Research: Solid Earth*, **101**, 3139–3156, https://doi.org/10.1029/95JB03446

Christensen, N.I. 2004. Serpentinites, peridotites, and seismology. *International Geology Review*, **46**, 795–816, https://doi.org/10.2747/0020-6814.46.9.795

Christensen, N.I. and Mooney, W.D. 1995. Seismic velocity structure and composition of the continental crust: a global view. *Journal of Geophysical Research: Solid Earth*, **100**, 9761–9788, https://doi.org/10.1029/95JB00259

Cooper Boemmels, J. 2020. *Postrift Development of the Eastern North American Margin: Early Cretaceous Intraplate Magmatism and Normal Faulting of Western Vermont and Eastern New York*. PhD Thesis, University of Connecticut, https://digitalcommons.lib.uconn.edu/dissertations/2609

Crotwell, H.P. and Owens, T.J. 2005. Automated receiver function processing. *Seismological Research Letters*, **76**, 702–709, https://doi.org/10.1785/gssrl.76.6.702

De Souza, S., Tremblay, A., Ruffet, G. and Pinet, N. 2012. Ophiolite obduction in the Quebec Appalachians, Canada – $^{40}Ar/^{39}Ar$ age constraints and evidence for syn-tectonic erosion and sedimentation. *Canadian Journal of Earth Sciences*, **49**, 91–110, https://doi.org/10.1139/e11-037

Durrheim, R.J. and Mooney, W.D. 1991. Archean and Proterozoic crustal evolution: evidence from crustal seismology. *Geology*, **19**, 606–609, https://doi.org/10.1130/0091-7613(1991)019<0606:AAPCEE>2.3.CO;2

Eaton, D.W. and Frederiksen, A. 2007. Seismic evidence for convection-driven motion of the North American plate. *Nature*, **446**, 428–431, https://doi.org/10.1038/nature05675

Evans, R.L., Benoit, M.H., Long, M.D., Elsenbeck, J., Ford, H.A., Zhu, J. and Garcia, X. 2019. Thin lithosphere beneath the central Appalachian Mountains: a combined seismic and magnetotelluric study. *Earth and Planetary Science Letters*, **519**, 308–316, https://doi.org/10.1016/j.epsl.2019.04.046

Ford, H.A., Long, M.D. and Wirth, E.A. 2016. Midlithospheric discontinuities and complex anisotropic layering in the mantle lithosphere beneath the Wyoming and Superior provinces. *Journal of Geophysical Research: Solid Earth*, **121**, 6675–6697, https://doi.org/10.1002/2016JB012978

Ganne, J., Feng, X. *et al*. 2018. When Proterozoic crusts became thick: new insights from magma petrology. *Geosciences*, **8**, 428, https://doi.org/10.3390/geosciences8120428

Goldhagen, G.B., Ford, H.A. and Long, M.D. 2022. Evidence for a lithospheric step and pervasive lithospheric thinning beneath southern New England, northeastern USA. *Geology*, **50**, 1078–1082, https://doi.org/10.1130/G50133.1

Hatcher, R.D., Jr 2005. Southern and central Appalachians. *Encyclopedia of Geology*, 72–81, https://doi.org/10.1016/B0-12-369396-9/00408-1

Hatcher, R.D. 2010. The Appalachian orogen: a brief summary. *Geological Society of America Memoir*, **206**, 1–19, https://doi.org/10.1130/2010.1206(01)

Hillenbrand, I.W. and Williams, M.L. 2021. Paleozoic evolution of crustal thickness and elevation in the northern Appalachian orogen, USA. *Geology*, **49**, 946–951, https://doi.org/10.1130/G48705.1

Hillenbrand, I.W., Williams, M.L., Li, C. and Gao, H. 2021. Rise and fall of the Acadian altiplano: evidence for a Paleozoic orogenic plateau in New England. *Earth and Planetary Science Letters*, **560**, 116797, https://doi.org/10.1016/j.epsl.2021.116797

Hillenbrand, I., Williams, M.L., Jercinovic, M.J., Heizler, M.T. and Tjapkes, D.J. 2022. Petrochronologic constraints on Paleozoic tectonics in southern New England. *Geological Society of America Memoirs*, **220**, https://doi.org/10.1130/2022.1220(25)

Hillenbrand, I.W., Williams, M.L., Peterman, E.M., Jercinovic, M.J. and Dietsch, C.W. 2023. Petrochronologic constraints on inverted metamorphism, terrane accretion, thrust stacking, and ductile flow in the Gneiss Dome belt, northern Appalachian orogen. *Journal of Metamorphic Geology*, **41**, 1197–1235, https://doi.org/10.1111/jmg.12741

Holbrook, W.S., Mooney, W.D. and Christensen, N.I. 1992. The seismic velocity structure of the deep continental crust. *Continental Lower Crust*, **23**, 1–43.

Hughes, S. and Luetgert, J.H. 1991. Crustal structure of the western New England Appalachians and the Adirondack Mountains. *Journal of Geophysical Research: Solid Earth*, **96**, 16471–16494, https://doi.org/10.1029/91JB01657

Hughes, S., Luetgert, J.H. and Christensen, N.I. 1993. Reconciling deep seismic refraction and reflection data from the Grenvillian-Appalachian boundary in western New England. *Tectonophysics*, **225**, 255–269, https://doi.org/10.1016/0040-1951(93)90301-Y

Hynes, A. and Rivers, T. 2010. Protracted continental collision – evidence from the Grenville orogen. *Canadian Journal of Earth Sciences*, **47**, 591–620, https://doi.org/10.1139/E10-003

IRIS, DMC 2010. Data services products: EARS EarthScope automated receiver survey.

IRIS Transportable Array 2003. USArray transportable array [dataset]. International Federation of Digital Seismograph Networks, https://doi.org/10.7914/SN/TA

Isachsen, Y.W. 1975. Possible evidence for contemporary doming of the Adirondack Mountains, New York, and suggested implications for regional tectonics and seismicity. *Tectonophysics*, **29**, 169–181, https://doi.org/10.1016/0040-1951(75)90142-0

Julien, P.S. and Hubert, C. 1975. Evolution of the Taconian orogen in the Quebec Appalachians. *American Journal of Science*, **275**, 337–362.

Karabinos, P., Macdonald, F.A. and Crowley, J.L. 2017. Bridging the gap between the foreland and hinterland I: geochronology and plate tectonic geometry of Ordovician magmatism and terrane accretion on the Laurentian margin of New England. *American Journal of Science*, **317**, 515–554, https://doi.org/10.2475/05.2017.01

Kern, H. and Tubia, J.M. 1993. Pressure and temperature dependence of P- and S-wave velocities, seismic anisotropy and density of sheared rocks from the Sierra

Alpujata massif (Ronda peridotites, southern Spain). *Earth and Planetary Science Letters*, **119**, 191–205, https://doi.org/10.1016/0012-821X(93)90016-3

Kinney, S.T., MacLennan, S.A., Keller, C.B., Schoene, B., Setera, J.B., VanTongeren, J.A. and Olsen, P.E. 2021. Zircon U–Pb geochronology constrains continental expression of Great Meteor Hotspot magmatism. *Geophysical Research Letters*, **48**, e2020GL091390, https://doi.org/10.1029/2020GL091390

Krivoruchko, K. 2012. Empirical Bayesian kriging. *ArcUser Fall*, **6**, 1145, https://www.esri.com/news/arcuser/1012/empirical-byesian-kriging.html

Langston, C.A. 1977. The effect of planar dipping structure on source and receiver responses for constant ray parameter. *Bulletin of the Seismological Society of America*, **67**, 1029–1050.

Levin, V., Lerner-Lam, A. and Menke, W. 1995*a*. Anomalous mantle structure at the Proterozoic–Paleozoic boundary in northeastern US. *Geophysical Research Letters*, **22**, 121–124, https://doi.org/10.1029/94GL02693

Levin, V., Kim, W.-Y. and Menke, W. 1995*b*. Seismic velocities in the shallow crust of western New England and northern New York. *Bulletin of the Seismological Society of America*, **85**, 207–219.

Levin, V., Park, J., Brandon, M.T. and Menke, W. 2000. Thinning of the upper mantle during late Paleozoic Appalachian orogenesis. *Geology*, **28**, 239–242, https://doi.org/10.1130/0091-7613(2000)28<239:TOTUMD>2.0.CO;2

Levin, V., VanTongeren, J.A. and Servali, A. 2016. How sharp is the sharp Archean Moho? Example from eastern Superior Province. *Geophysical Research Letters*, **43**, 1928–1933, https://doi.org/10.1002/2016GL067729

Levin, V., Servali, A., VanTongeren, J., Menke, W. and Darbyshire, F. 2017. Crust–mantle boundary in eastern North America, from the (oldest) craton to the (youngest) rift. *Geological Society of America, Special Papers*, **526**, https://doi.org/10.1130/2017.2526(06)

Levin, V., Long, M.D., Skryzalin, P., Li, Y. and López, I. 2018. Seismic evidence for a recently formed mantle upwelling beneath New England. *Geology*, **46**, 87–90, https://doi.org/10.1130/G39641.1

Li, C., Gao, H., Williams, M.L. and Levin, V. 2018. Crustal thickness variation in the northern Appalachian Mountains: implications for the geometry of 3-D tectonic boundaries within the crust. *Geophysical Research Letters*, **45**, 6061–6070, https://doi.org/10.1029/2018GL078777

Li, C., Gao, H. and Williams, M.L. 2020. Seismic characteristics of the eastern North American crust with Ps converted waves: terrane accretion and modification of continental crust. *Journal of Geophysical Research: Solid Earth*, **125**, e2019JB018727, https://doi.org/10.1029/2019JB018727

Li, C., Hibbard, L., Gao, H. and Williams, M.L. 2023. Seismic evidence for metamorphic densification of the lower continental crust in eastern North America. *Journal of Geophysical Research: Solid Earth*, **128**, e2023JB026602, https://doi.org/10.1029/2023JB026602

Li, Y., Levin, V., Elkington, S. and Hlavaty, J. 2019. Localized anisotropic domains beneath eastern North America. *Geochemistry, Geophysics, Geosystems*, **20**, 5499–5521, https://doi.org/10.1029/2019GC008518

Li, Y., Levin, V., Nikulin, A. and Chen, X. 2021. Systematic mapping of upper mantle seismic discontinuities beneath northeastern North America. *Geochemistry, Geophysics, Geosystems*, **22**, e2021GC009710, https://doi.org/10.1029/2021GC009710

Li, Z.-X., Bogdanova, S.V. *et al*. 2008. Assembly, configuration, and break-up history of Rodinia: a synthesis. *Precambrian Research*, **160**, 179–210, https://doi.org/10.1016/j.precamres.2007.04.021

Link, F., Rümpker, G. and Kaviani, A. 2020. Simultaneous inversion for crustal thickness and anisotropy by multiphase splitting analysis of receiver functions. *Geophysical Journal International*, **223**, 2009–2026, https://doi.org/10.1093/gji/ggaa435

Link, F., Reiss, M.C. and Rümpker, G. 2022. An automatized XKS-splitting procedure for large data sets: extension package for SplitRacer and application to the USArray. *Computers & Geosciences*, **158**, 104961, https://doi.org/10.1016/j.cageo.2021.104961

Linkimer, L., Beck, S.L., Schwartz, S.Y., Zandt, G. and Levin, V. 2010. Nature of crustal terranes and the Moho in northern Costa Rica from receiver function analysis. *Geochemistry, Geophysics, Geosystems*, **11**, https://doi.org/10.1029/2009GC002795

Long, M.D. and Aragon, J.C. 2020. Probing the structure of the crust and mantle lithosphere beneath the southern New England Appalachians via the SEISConn deployment. *Seismological Society of America*, **91**, 2976–2986, https://doi.org/10.1785/0220200163

Long, M.D., Benoit, M.H., Aragon, J.C. and King, S.D. 2019. Seismic imaging of mid-crustal structure beneath central and eastern North America: possibly the elusive Grenville deformation? *Geology*, **47**, 371–374, https://doi.org/10.1130/G46077.1

Long, M.D., Benoit, M.H., Evans, R.L., Aragon, J.C. and Elsenbeck, J. 2020. The MAGIC experiment: a combined seismic and magnetotelluric deployment to investigate the structure, dynamics, and evolution of the central Appalachians. *Seismological Research Letters*, **91**, 2960–2975, https://doi.org/10.1785/0220200150

Lund, K., Box, S.E. *et al*. 2015. *Basement Domain Map of the Conterminous United States and Alaska*. US Geological Survey, Data Series 898.

Luo, Y., Long, M.D. *et al*. 2021. High-resolution P_s receiver function imaging of the crust and mantle lithosphere beneath southern New England and tectonic implications. *Journal of Geophysical Research: Solid Earth*, **126**, e2021JB022170, https://doi.org/10.1029/2021JB022170

Luo, Y., Long, M.D., Rondenay, S., Karabinos, P. and Kuiper, Y.D. 2022. Wavefield migration imaging of Moho geometry and upper mantle structure beneath southern New England. *Geophysical Research Letters*, **49**, e2022GL099013, https://doi.org/10.1029/2022GL099013

Luo, Y., Long, M.D., Karabinos, P., Rondenay, S. and Masis Arce, R. 2023*a*. First-order transition in Appalachian orogenic processes revealed by along-strike variation of the Moho geometry. *Journal of Geophysical Research: Solid Earth*, **128**, e2023JB027024, https://doi.org/10.1029/2023JB027024

Luo, Y., Long, M.D., Link, F., Karabinos, P. and Kuiper, Y.D. 2023*b*. Insights from layered anisotropy beneath southern New England: from ancient tectonism to

present-day mantle flow. *Geochemistry, Geophysics, Geosystems*, **24**, e2023GC011118, https://doi.org/10.1029/2023GC011118

Macdonald, F.A., Ryan-Davis, J., Coish, R.A., Crowley, J.L. and Karabinos, P. 2014. A newly identified Gondwanan terrane in the northern Appalachian Mountains: implications for the Taconic orogeny and closure of the Iapetus Ocean. *Geology*, **42**, 539–542, https://doi.org/10.1130/G35659.1

Masis, R., Long, M.D., Karabinos, P. and Bourke, J. 2024. Lithospheric structure in the northern Appalachian Mountains: a detailed examination of the abrupt change in crustal thickness in northwestern Massachusetts. *Geochemistry, Geophysics, Geosystems*, **25**, e2024GC011570, https://doi.org/10.1029/2024GC011570

Mazza, S.E., Gazel, E., Johnson, E.A., Bizimis, M., McAleer, R. and Biryol, C.B. 2017. Post-rift magmatic evolution of the eastern North American 'passive-aggressive' margin. *Geochemistry, Geophysics, Geosystems*, **18**, 3–22, https://doi.org/10.1002/2016GC006646

McLelland, J.M., Selleck, B.W. and Bickford, M.E. 2010. Review of the Proterozoic evolution of the Grenville Province, its Adirondack outlier, and the Mesoproterozoic inliers of the Appalachians. *Geological Society of America, Memoirs*, **206**, 21–49, https://doi.org/10.1130/2010.1206(02)

McLelland, J.M., Selleck, B.W. and Bickford, M.E. 2013. Tectonic evolution of the Adirondack Mountains and Grenville orogen inliers within the USA. *Geoscience Canada*, **40**, 318–352, https://doi.org/10.12789/geocanj.2013.40.022

Murodov, D., Mi, W., Murodov, A., Oimuhmmadzoda, I., Abdulov, S. and Xin, W. 2022. Deep crustal structure beneath the Pamir–Tibetan Plateau: insights from the Moho depth and V_p/V_s ratio variation. *Frontiers in Earth Science*, **10**, 821497, https://doi.org/10.3389/feart.2022.821497

Musacchio, G., Mooney, W.D., Luetgert, J.H. and Christensen, N.I. 1997. Composition of the crust in the Grenville and Appalachian provinces of North America inferred from V_p/V_s ratios. *Journal of Geophysical Research: Solid Earth*, **102**, 15225–15241, https://doi.org/10.1029/96JB03737

Náběl ek, J., Hetenyi, G. *et al.* 2009. Underplating in the Himalaya–Tibet collision zone revealed by the Hi-CLIMB experiment. *Science (New York)*, **325**, 1371–1374, https://doi.org/10.1126/science.1167719

Olugboji, T.M. and Park, J. 2016. Crustal anisotropy beneath Pacific Ocean-islands from harmonic decomposition of receiver functions. *Geochemistry, Geophysics, Geosystems*, **17**, 810–832, https://doi.org/10.1002/2015GC006166

Park, J. and Levin, V. 2000. Receiver functions from multiple-taper spectral correlation estimates. *Bulletin of the Seismological Society of America*, **90**, 1507–1520, https://doi.org/10.1785/0119990122

Park, J. and Levin, V. 2016. Anisotropic shear zones revealed by backazimuthal harmonics of teleseismic receiver functions. *Geophysical Supplements to the Monthly Notices of the Royal Astronomical Society*, **207**, 1216–1243, https://doi.org/10.1093/gji/ggw323

Ratcliffe, N.M., Stanley, R.S., Gale, M.H., Thompson, P.J. and Walsh, G.J. 2011. *Bedrock Geologic Map of Vermont, 1:100 000 scale*. US Geological Survey Scientific Investigations Map, 3184.

Rivers, T. 2008. Assembly and preservation of lower, mid, and upper orogenic crust in the Grenville Province – Implications for the evolution of large hot long-duration orogens. *Precambrian Research*, **167**, 237–259, https://doi.org/10.1016/j.precamres.2008.08.005

Rivers, T. 2015. Tectonic setting and evolution of the Grenville Orogen: an assessment of progress over the last 40 years. *Geoscience Canada*, **42**, 77–124, https://doi.org/10.12789/geocanj.2014.41.057

Rudnick, R.L. and Fountain, D.M. 1995. Nature and composition of the continental crust: a lower crustal perspective. *Reviews of Geophysics*, **33**, 267–309, https://doi.org/10.1029/95RG01302

Ryan, W.B.F., Carbotte, S.M. *et al.* 2009. Global Multi-Resolution Topography (GMRT) synthesis data set. *Geochemistry Geophysics Geosystems*, **10**, QQ03014, https://doi.org/10.1029/2008GC002332

Schulte-Pelkum, V. and Mahan, K.H. 2014. A method for mapping crustal deformation and anisotropy with receiver functions and first results from USArray. *Earth and Planetary Science Letters*, **402**, 221–233, https://doi.org/10.1016/j.epsl.2014.01.050

Shen, W. and Ritzwoller, M.H. 2016. Crustal and uppermost mantle structure beneath the United States. *Journal of Geophysical Research: Solid Earth*, **121**, 4306–4342, https://doi.org/10.1002/2016JB012887

Shiomi, K. and Park, J. 2008. Structural features of the subducting slab beneath the Kii Peninsula, central Japan: seismic evidence of slab segmentation, dehydration, and anisotropy. *Journal of Geophysical Research: Solid Earth*, **113**, https://doi.org/10.1029/2007JB005535

Stanley, R.S. and Ratcliffe, N.M. 1985. Tectonic synthesis of the Taconian orogeny in western New England. *Geological Society of America Bulletin*, **96**, 1227–1250, https://doi.org/10.1130/0016-7606(1985)96<1227:TSOTTO>2.0.CO;2

Stanley, R.S., Roy, D.L., Hatch, N.L. and Knapp, D.A. 1984. Evidence for tectonic emplacement of ultramafic and associated rocks in the pre-Silurian eugeoclinal belt of western New England; vestiges of an ancient accretionary wedge. *American Journal of Science*, **284**, 559–595, https://doi.org/10.2475/ajs.284.4-5.559

Swenson, J.B., Voller, V.R., Paola, C., Parker, G. and Marr, J.G. 2000. Fluvio-deltaic sedimentation: a generalized Stefan problem. *European Journal of Applied Mathematics*, **11**, 433–452, https://doi.org/10.1017/S0956792500004198

Tesauro, M., Kaban, M.K., Mooney, W.D. and Cloetingh, S.A.P.L. 2014. Density, temperature, and composition of the North American lithosphere – new insights from a joint analysis of seismic, gravity, and mineral physics data: 2. Thermal and compositional model of the upper mantle. *Geochemistry, Geophysics, Geosystems*, **15**, 4808–4830, https://doi.org/10.1002/2014GC005484

Trabant, C., Hutko, A.R., Bahavar, M., Karstens, R., Ahern, T. and Aster, R. 2012. Data products at the IRIS DMC: stepping stones for research and other applications. *Seismological Research Letters*, **83**, 846–854, https://doi.org/10.1785/0220120032

Tremblay, A. and Castonguay, S. 2002. Structural evolution of the Laurentian margin revisited (southern Quebec Appalachians): implications for the Salinian orogeny and successor basins. *Geology*, **30**, 79–82, https://doi.org/10.1130/0091-7613(2002)030<0079:SEOTLM>2.0.CO;2

Tremblay, A. and Pinet, N. 2016. Late Neoproterozoic to Permian tectonic evolution of the Quebec Appalachians, Canada. *Earth-Science Reviews*, **160**, 131–170, https://doi.org/10.1016/j.earscirev.2016.06.015

Tremblay, A., Ruffet, G. and Bédard, J.H. 2011. Obduction of Tethyan-type ophiolites – a case-study from the Thetford-Mines ophiolitic Complex, Quebec Appalachians, Canada. *Lithos*, **125**, 10–26, https://doi.org/10.1016/j.lithos.2011.01.003

van Staal, C.R., Whalen, J.B., Valverde-Vaquero, P., Zagorevski, A. and Rogers, N. 2009. Pre-Carboniferous, episodic accretion-related, orogenesis along the Laurentian margin of the northern Appalachians. *Geological Society, London, Special Publications*, **327**, 271–316, https://doi.org/10.1144/SP327.13

Viegas, G.M., Baise, L.G. and Abercrombie, R.E. 2010. Regional wave propagation in New England and New York. *Bulletin of the Seismological Society of America*, **100**, 2196–2218, https://doi.org/10.1785/0120090223

Wagner, L.S., Stewart, K. and Metcalf, K. 2012. Crustal-scale shortening structures beneath the Blue Ridge Mountains, North Carolina, USA. *Lithosphere*, **4**, 242–256, https://doi.org/10.1130/L184.1

Wessel, P., Smith, W.H.F., Scharroo, R., Luis, J. and Wobbe, F. 2013. Generic mapping tools: improved version released. *Eos, Transactions American Geophysical Union*, **94**, 409–410, https://doi.org/10.1002/2013EO450001

Whitehead, J., Reynolds, P.H. and Spray, J.G. 1995. The sub-ophiolitic metamorphic rocks of the Québec Appalachians. *Journal of Geodynamics*, **19**, 325–350, https://doi.org/10.1016/0264-3707(94)00021-M

Whitehead, J., Reynolds, P.H. and Spray, J.G. 1996. $^{40}Ar/^{39}Ar$ age constraints on Taconian and Acadian events in the Quebec Appalachians. *Geology*, **24**, 359–362, https://doi.org/10.1130/0091-7613(1996)024<0359:AAACOT>2.3.CO;2

Whitehead, J., Dunning, G.R. and Spray, J.G. 2000. U–Pb geochronology and origin of granitoid rocks in the Thetford Mines ophiolite, Canadian Appalachians. *Geological Society of America Bulletin*, **112**, 915–928, https://doi.org/10.1130/0016-7606(2000)112<915:UGAOOG>2.0.CO;2

Wilson, J.T. 1966. Did the Atlantic close and then re-open? *Nature*, **211**, 676–681.

Withjack, M.O. and Schlische, R.W. 2005. A review of tectonic events on the passive margin of eastern North America. *SEPM Gulf Coast Section Publications*, **25**, https://doi.org/10.5724/gcs.05.25.0203

Yang, X. and Gao, H. 2018. Full-wave seismic tomography in the northeastern United States: new insights into the uplift mechanism of the Adirondack Mountains. *Geophysical Research Letters*, **45**, 5992–6000, https://doi.org/10.1029/2018GL078438

Zandt, G., Velasco, A.A. and Beck, S.L. 1994. Composition and thickness of the southern Altiplano crust, Bolivia. *Geology*, **22**, 1003–1006, https://doi.org/10.1130/0091-7613(1994)022<1003:CATOTS>2.3.CO;2

Zhu, L. and Kanamori, H. 2000. Moho depth variation in southern California from teleseismic receiver functions. *Journal of Geophysical Research: Solid Earth*, **105**, 2969, https://doi.org/10.1029/1999JB900322